SEISMICITY OF THE BATH COUNTY, VIRGINIA LOCALE

by

Eric Donald Todd

Thesis submitted to the Faculty of the
Virginia Polytechnic Institute and State University
in partial fulfillment of the requirements for the degree of
MASTER OF SCIENCE
in
GEOPHYSICS

APPROVED:

G. A. Bollinger (Chairman)

J. A. Snoke

E. S. Robinson

December, 1982
Blacksburg, Virginia

ERRATA

We are embarrassed by the presence and number of these typographical errors. This is an example of what can happen when a word-processor is used and the final draft is not checked prior to printing--GAB.

Page	Paragraph	Line	Change	To
ii	1	11	particlular	particular
v		No. 14	Outiside	Outside
v		Last	PolarityData	Polarity Data
4	2	2	Electic	Electric
4	2	5	resevoirs	reservoirs (throughout paper)
4	3	6	studiedmore	studied more
11	3	6	wasso	was so
13	2	6	amd	and
13	2	11	Costain et al., in 1977.	Perry et al. (1979).
13	2	14,15	Costain and his co-authors (after Reeves, 1932)	Perry et al. (1979)
13	2	16,17	gradient. The heated water then migrates through permeable layers to the surface	gradient, and that transverse (E-W) fracture zones are an important component of their model
19	1	5	5.450.09	5.45 ± 0.09
19	1	6	3.090.10	3.09 ± 0.10
19	3	2	6.041.71	6.04 ± 1.71
24		Last	tt	TT
26	Caption	5	leastsquares	least squares
30	2	10	6.530.22	6.53 ± 0.22
			3.840.08	3.84 ± 0.08
		12	8.180.11	8.18 ± 0.11
			4.790.15	4.79 ± 0.15
		14	8.110.19	8.11 ± 0.19
33	1	8	5.41.12	5.41 ± 0.12
		9	5.350.06	5.35 ± 0.06
40	1	6	were	was
	2	8	were	was
44	2	1	Hypoellipse	HYPOELLIPSE
48	Table 3	All		± signs missing in all columns. The last row (Ave) should read: 0.23 ± 66.0, 0.45 ± 30.0, 0.5 ± 25.3, 0.8 ± 65.9, 0.8 ± 8.9
51	1	2	Outiside	Outside
54	Table 6	All		± signs missing in all columns. The last row (Ave) should read: 1.4 ± 28.2, 6.5 ± 4.0, 11.0 ± 1.5, 12.2 ± 6.2, 1.0 ± 11.3
55	Table 7	Last		Move complete line 6 spaces to the left
58	2	5	si	is
60	3	8,9	were	was
71	3	1	asumptions	assumptions
73	2	3	are	is
74	Caption	2	PolarityData	Polarity Data
87	1	3	predominately	predominantly
	2	11	predominately	predominantly
102	2	9	model	models

ACKNOWLEDGMENTS

I wish to first thank Dr. G. A. Bollinger, whose moral and financial support were so important to me. Due to his advice and guidance I reached a level of professionalism that would have been impossible on my own. Dr. J. A. Snoke made several excellent suggestions and helped me with many programming problems. I am deeply indebted to these two men. I also wish to thank Dr. E. S. Robinson for his critical reading of this thesis. In addition, I would like to thank Dr. L. T. Long at Georgia Tech for supplying me with the focal mechanism program and answering my questions about it. I wish to thank Vepco for their co-operation and financial support during this study. In particlular, Mr. D. A. Mangun was very helpful and showed great interest in this project. Thanks also go to Mr. Thomas Boyd, Mr. Thomas Pratt, Mr. Matt Sibol and Mr. Mark Gresko for their friendship, suggestions and help and Ms. Debra A. Bender and Ms. Janice C. Crowe for their work in editing this paper. Finally, I wish to thank my parents who instilled in me the love of learning and desire to succeed that has sustained me during this project. The lessons they taught me by example have served me well during my lifetime. Their support is most appreciated.

This research was sponsored in part by the Nuclear Regulatory Commission Contract No. NRC-04-77-134, Mod. 6 and 7 and in part by the National Science Foundation Grant NSF#EAR-7923766.

TABLE OF CONTENTS

LIST OF TABLES

LIST OF FIGURES

Chapter I

THE BATH COUNTY AREA

Bath County, bordered by Highland, Rockbridge and Alleghany Counties, Virginia and by Pocahontas County, West Virginia, is one of the westernmost counties in Virginia and is located in the Valley and Ridge province. The linear ridges and intervening valleys create the distinctive topography of the province. The county is sparsely populated, with 5,776 people (1980 census) located in the county's 540,000 square miles.

Bath County is within the largest concentration of thermal springs in the Eastern United States (Figure 1). There are several well-known resorts built around those thermal springs. The county is named after the town of Bath, in England, also a site of thermal springs.

This area of thermal springs concentration is geophysically anomalous for several reasons. First, it had very low-level intensity response to the Charleston, South Carolina earthquake of 1886 (Dutton, 1889; Figure 2). Though the intensity data were sparse in the West Virginia-Western Virginia area, Dutton felt that they were indicating an area of lowered intensity. Independent re-evaluation of Dutton's intensity data by three seismologists has confirmed the existence of the low intensity zone in the Virginia-West Virginia area (Bollinger, 1977). Secondly, the area is the center of a broad, regional negative Bouguer Gravity anomaly (Kulander and Dean, 1978). Finally, the area is a se-

Figure 1: Map of Thermal Springs in the Eastern United States

Map of the Eastern United States showing the distribution of thermal springs. The numerals inside the state outlines denote the number of thermal springs in that state and shaded areas thermal spring concentrations. The star shows the location of Hot Springs, Virginia, located in Bath County. Note that the Bath County area is located in the largest concentration of thermal springs in the Eastern United States. (from Bollinger and Gilbert, 1974)

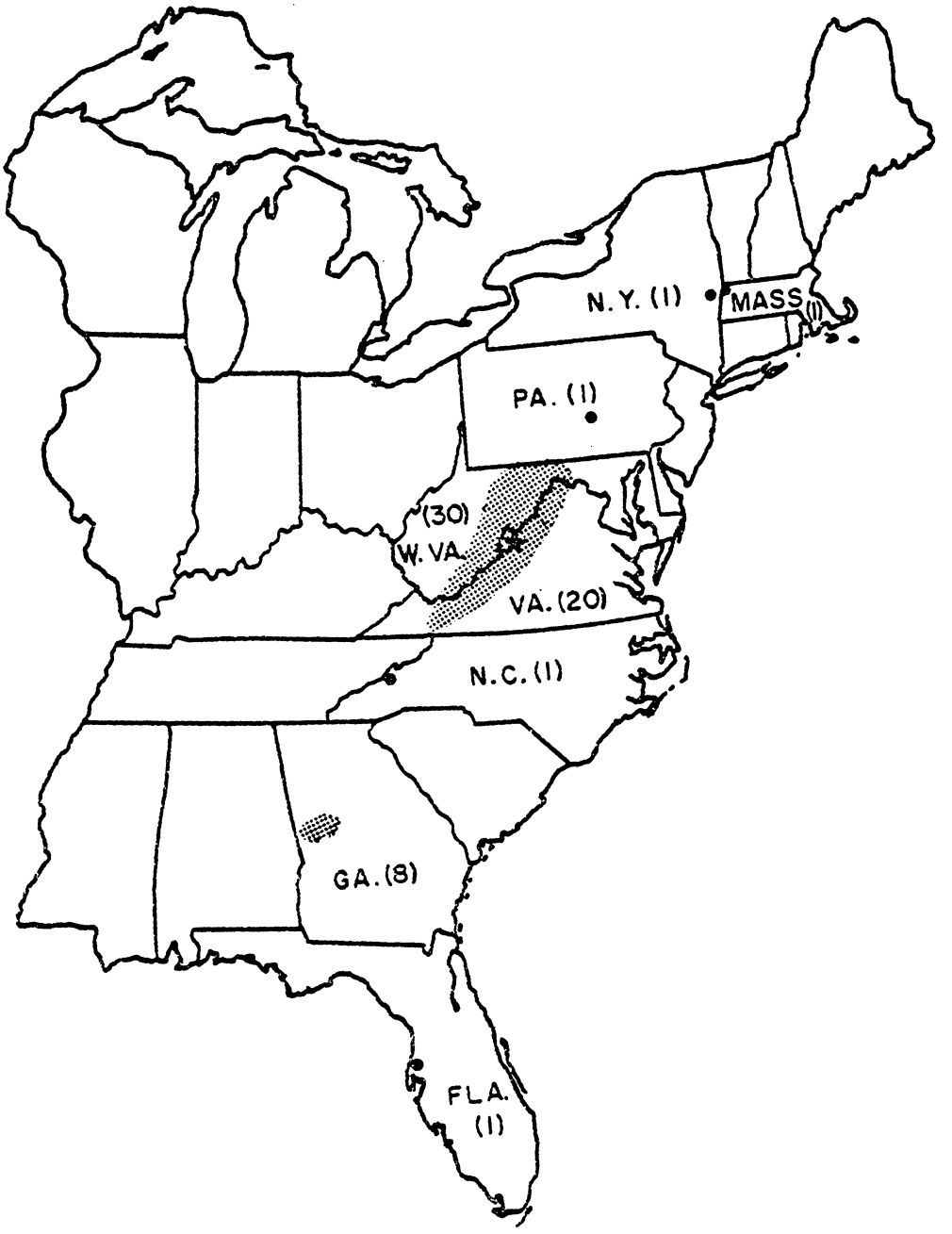
N.Y. (1)
MASS (1)
PA. (1)
(30)
W. VA.
VA. (20)
N.C. (1)
GA. (8)
FLA.
(1)

ismically quiescent locale in the otherwise active Appalachian Mountain chain (Bollinger and Gilbert, 1974). There is no record of historical seismicity in the study area. However, to the immediate north, south and east there is reported seismicity dating back to the 1700's.

The study area also attracts attention for engineering reasons. In Bath County, Virginia Electic and Power Company (Vepco) is constructing a 2100 megawatt hydroelectric project. It will operate on the principle of pumped-storage. The major engineering features of the project are two resevoirs behind earth- and rock-fill dams, a system of tunnels connecting the resevoirs and a powerhouse (Figure 3). The dam on the upper resevoir, at 460 feet high, will be the tallest dam of its type east of the Mississippi River. The water depths will be approximately 425 feet for the upper resevoir and 120 feet for the lower resevoir. During the generating cycle, the water level will vary by 105 feet in the upper resevoir and 60 feet in the lower. The project is scheduled for completion in 1986.

A principal objective of this study will be an analysis of the present (pre-resevoir filling) seismicity. An analysis of the frequency and size of earthquakes before resevoir filling is important in order to have a basis for comparison with any post resevoir filling seismicity. With such baseline data, any effects of the resevoirs on the local seismicity can be studiedmore effectively (Richter, 1957; Simpson, 1976; Lee and Stuart, 1980).

Figure 2: Intensity Map of 1886 Charleston, South Carolina Earthquake

Isoseismal map of the 1886 Charleston, South Carolina earthquake, after Dutton (1889). The shaded area indicates the location of the thermal springs concentration in Virginia and West Virginia from Figure 1. (from Bollinger and Gilbert, 1974)

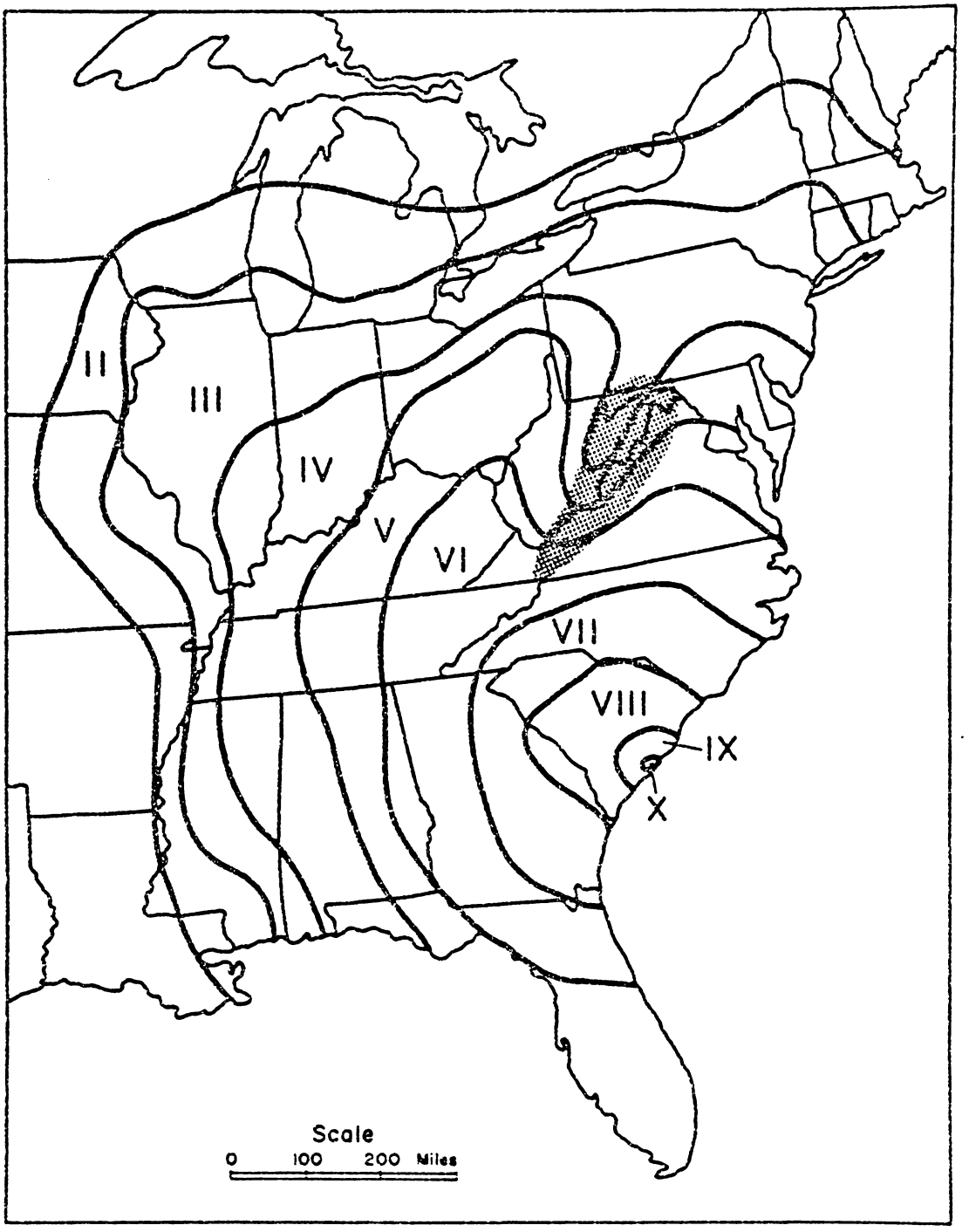

ISOSEISMAL MAP (Rossi-Forel), from Dutton, 1889

Rossi-Forel	X	IX+	VIII+ -IX-	VIII	VI-VII	V-VI	IV-V	III	I-II
Mod, Mercalli	X	IX	VIII	VII	VI	V	IV	III	II

Figure 3: Vepco Bath County Pumped-Storage Project

Map view of Vepco Bath County Pumped-Storage Project showing major engineering features. The upper dam (460 feet high) is in the upper center of the figure. The lower dam and the powerhouse are in the lower center of the figure. The water tunnels (labeled Water Conduits) connect the Upper and Lower Resevoir. There is approximately 1,100 feet of relief between the the two resevoirs.

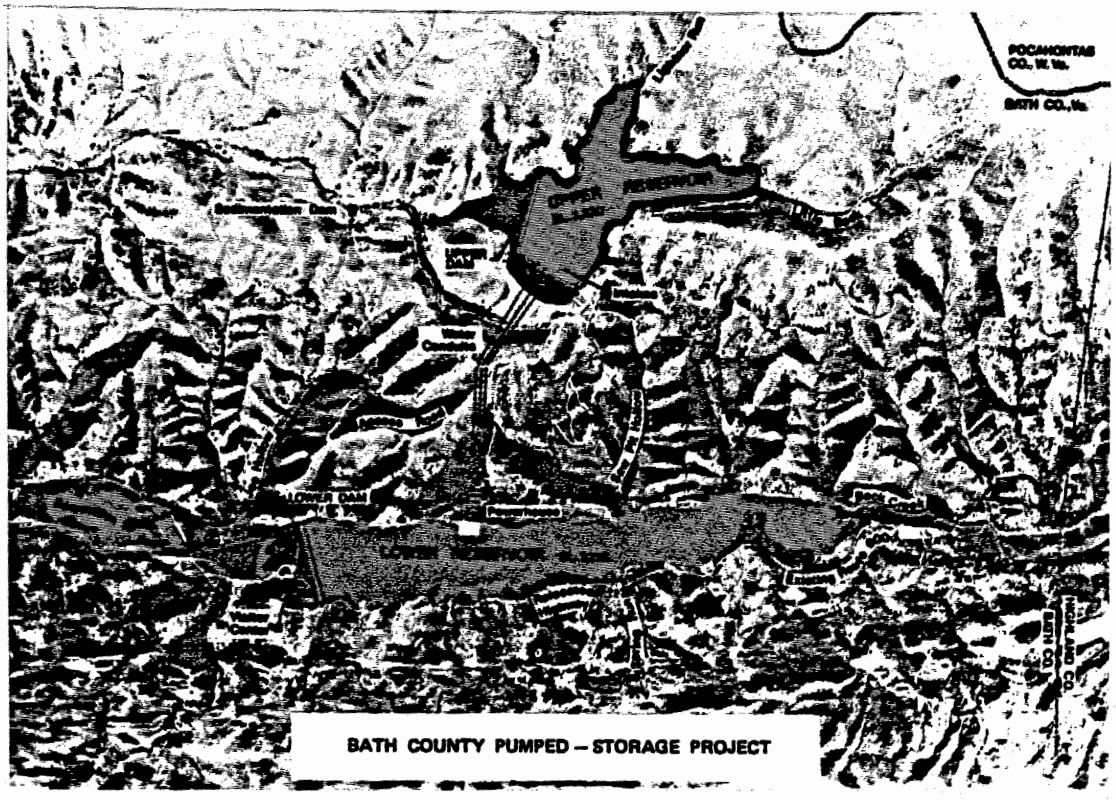

BATH COUNTY PUMPED – STORAGE PROJECT

To collect the background seismicity data, Vepco installed a 4 station microearthquake monitoring network in November, 1978. The network stations consist of Mark Products 1 Hz vertical seismometers and Sprengnether telemetry components. The seismic signals are carried by telephone line to Blacksburg, Virginia where they are recorded at the Virginia Tech Seismological Observatory. The network has an aperture of 25 km with a central station near the Vepco Bath County Pumped Storage Project. The stations are referred to by their 3 character codes, BV1, BV2, BV3 and BV4 (Figure 12).

This study of the seismicity of the Bath County area is in three main parts. First, a crustal velocity model for the Bath County area was developed. This model was developed by the method of refraction seismology using construction blasts on the Vepco project as a source. Next, the locational capability of the Bath County Seismic Network was tested by locating quarry and construction blasts and comparing those locations with the actual locations. Finally, the earthquakes recorded by the network were analyzed.

1.1 GEOLOGIC SUMMARY

Bath County encompasses 1,400 square km in Western Virginia. It extends from latitude 37 degrees 45 minutes to 38 degrees 15 minutes and from longitude 79 degrees 30 minutes to 80 degrees 5 minutes. The county is in the Valley and Ridge Province of Virginia. The elevation ranges from 480 meters to 1,160 meters above sea-level. The following geologic summary is adapted from Colton (1970).

The geologic history of the modern Valley and Ridge Province starts with the development of the Appalachian Basin. That basin was an elongate downwarp in the Pre-Cambrian crystalline rocks into which thick sequences of sediments were deposited. Its trend closely followed the trend of the present Atlantic coastline. Deposition was more or less continuous from early Cambrian time to Pennsylvanian time. Basin subsidence appears to have kept pace with sedimentation as most of the rocks were deposited in shallow water. The clastic sequences in the basin are wedge shaped with the thickest part of the wedge near the source areas to the north or northeast. The sequence thicknesses given here are estimates of the values in the study area.

The Early Cambrian sequence lies unconformably on the crystalline basement rocks. It consists of 1.2 km of interbedded, fine-to-coarse grained clastic rocks. Above it is the Cambrian to Middle Ordovician carbonate sequence, consisting of 1.9 km of limestone and dolomite. Gentle uplift of the depositional surface caused an erosional disconformity between the Lower and Middle Ordovician rocks. Above this unit is the Late Ordovician clastics consisting of 600 meters of shale, siltstones and sandstone. Above that sequence is the Early Silurian clastics, composed of 150 meters of coarse grained clastic rocks. The next younger sequence is the Silurian-Devonian carbonates. It is approximately 360 meters thick. Overlying those carbonates is the thick sequence of Devonian clastic rocks composed of 2.3 km of interbedded shale, mudrock, siltstone and sandstone. The next younger units are

the coarse-to-fine grained, non-calcareous rocks of Mississippian and Pennsylvanian age, of undetermined thickness. The sediments in the Appalachian Basin reached an average total thickness on the order of 18 km.

In Late Paleozoic and Early Mesozoic time these sediments were subjected to profound deformation. In the Valley and Ridge province, this deformation took the form of large-scale folding and thrust-faulting along sole-fault detachments in less competent formations. These detachments permitted the crystalline basement to remain relatively undisturbed. This results in little correlation between surficial geology and the structure of the underlying basement. Erosion began as soon as deformation started and present topography is erosionally controlled. Structurally, the study area is dominated by the Warm Springs Anticline. This large fold exposes Cambrian Beekmantown Limestone in the core and the Devonian Brallier Formation on the flanks.

1.2 PREVIOUS WORK

There is little previous work on the seismicity of Bath County. A microearthquake reconnaissance survey in 1973 detected some microearthquake activity (Bollinger and Gilbert, 1974). This activity was recorded on only one instrument, and stopped before other instruments could be moved into the area. The senior author now feels the activity wasso few in numbers and of such low magnitude (less than -2) as to not be tectonically important (Bollinger, personal communication, 1982).

The Bath County area has been included in several regional studies. The areal geology was mapped by Butts (1933, 1940) in his study of the Appalachian Valley in Virginia. In a more recent study, the gravity, magnetics and structure of the study area were analyzed in a study of West Virginia and adjacent states (Kulander and Dean, 1978). Their gravity survey shows a broad, regional gravity low centered in the study area. This regional low corresponds spatially to the area of highest elevation and thickest crust in the central Appalachians (James, et al. 1968). The crustal thickness in this area is 50 km or more and James and his co-workers show that the surface elevations are isostatically overcompensated.

Kulander and Dean (1978) also modeled the two-dimensional gravity over the Warm Springs Anticline. The result of that modeling indicates that imbricate thrust faults in less competent formations are ramping up and stacking the rocks into tectonically thickened sections. The authors found excellent agreement between the calculated two-dimensional gravity variations caused by this thickening and the Bouguer anomaly profile across the Warm Springs Anticline. These results suggest that the crystalline basement is not directly involved in Appalachian deformation. Kulander and Dean (1978) also developed a map showing the depth to crystalline basement rocks in the West Virginia - Virginia area. They used a combination of methods including magnetics, well-tests and sedimentary thickness projections. Their depth-to-basement estimate in the study area averages 4.9 km (16,000 feet) beneath sea

level and is in a basement structure referred to as the Martinsburg trough.

The source of the heat for the thermal springs in the study area has long been a subject of debate. The presence of a large, negative Bouguer gravity anomaly in the same area as the thermal springs has led some to suggest that a large, still cooling pluton was responsible for both the temperature of the springs and the negative Bouguer anomaly (Dennison amd Johnson, 1971). In addition, it has been suggested that such a pluton would attenuate 2 to 10 second period surface waves and thereby be responsible for the anomalously low intensities reported in the Bath County area from the 1886 Charleston, South Carolina earthquake (Bollinger and Gilbert, 1974). A crustal heat flow measurement was subsequently obtained by Costain et al., in 1977. Their measurements showed no abnormal heat flows. That result eliminates the theory that a still cooling pluton is the major source of heat for the thermal springs. Costain and his co-authors (after Reeves, 1932) suggest that deep circulation of meteoric ground water raises the water temperature through the normal geothermal gradient. The heated water then migrates through permeable layers to the surface.

Chapter II

THE BATH COUNTY NETWORK CRUSTAL VELOCITY MODEL

To enable accurate event locations by the Bath County network, a velocity model was developed specifically for the network locale. The model was developed by the method of refraction seismology with construction blasts on the Vepco project serving as a source. The signals were recorded on mobile and fixed arrays. P and S wave arrival-times versus distance were analyzed for slope, intercept and uncertainties in those parameters by the method of least squares. In this chapter, the model is developed and then interpreted geologically.

2.1 FIELD PROCEDURES

Six portable seismographs (Sprengnether MEQ800 smoked paper recorders with Mark Products L4-C, 1 Hz vertical seismometers) were employed as a mobile array. The recorder clocks were syncronized to WWV every other day using a portable oscilloscope. Drift corrections averaged 0.02 seconds per day. Seismometers were buried so that they were at least 5 cm beneath the ground surface to insure good coupling and to reduce wind noise.

The recorder drums were operated at 60 mm/min with a trace spacing of 1 mm and a recording duration of 48 hours. The gain of the recorders varied from 72 dB to 84 dB, yielding 10 Hz magnifications from 139K to 540K. High/low pass filter settings were either 5 and 10 hz or

out and 10 hz. The single exception to these values was the origin-time recorder, sited within 250 meters of the blasts. Its gain was 60 dB (35k at 10 Hz) with filter settings of out and 5 Hz. This combination gave very impulsive origin-time readings with a minimum of background noise. The origin-time recorder drum speed was 120 mm/min with 1 mm trace spacing which yielded 24 hours recording duration and a reading accuracy of 0.05 seconds. The average clock drift corrections were 0.02 seconds per 24 hours, and therefore were neglected. As noted above, the origin-time seismometer was close enough to the blasts that the travel-time from the blast to the seismometer was roughly equal to the reading accuracy (250 meters/5450 meters/sec = 0.046 sec).

As previously mentioned, the fixed network stations consist of Mark Products L4-C seismometers with Sprengnether telemetry components. The signals are transmitted by telephone line to the Virginia Tech Seismological Observatory for recording. The visual recorders used at the Observatory are Sprengnether VR-60 pen-and-ink recorders running at 60 mm/min and with trace separation of 2.5 mm. This configuation yields approximately 24 hours of recording with a reading accuracy of 0.1 sec. Time is placed on the records by a Kinemetrics Model 468-DC Satellite clock. The constant time correction during the study was -0.017 seconds.

The locations of the portable stations were spotted on U.S.G.S. 7.5 minute topographic sheets. The error in location is estimated to be

about 30 meters (2 mm on the sheets), and therefore negligible. The source-to-receiver distances and azimuths were calculated by standard methods (Bullen, 1963). The portable station arrays were located in Bath County, Virginia and Pocahontas County, West Virginia.

A total of 39 construction blasts were monitored at 19 portable and 4 permanent sites. Four of the portable sites were either too noisy or too distant to provide accurate readings. It was determined during the experiment that, at distances greater than 35 km, signal attenuation would preclude accurate arrival-time determinations. Figure 4 gives the spatial distribution of the observing stations with respect to the blast site.

Multiple blasts (3 to 10) were recorded at each station in order to better establish the arrival-times. Travel-times were averaged and those more than 1 standard deviation from the mean to that station were eliminated from the data set and the final mean recalculated.

2.2 DISCRETE LAYER VELOCITY MODEL

The plot of Mean Travel-Time versus Distance (Figure 5) out to 40 km shows a 2 branch travel-time curve for P. The P crossover distance is between 20 and 30 km. The S crossover distance is not defined. (Appendix A contains all the travel-times calculated from the field records.) Reduced travel-time plots for the average of the P-wave travel-times were made for reducing velocities 5.0 km/sec and 6.0 km/sec (Figures 6 and 7). Note that the arrivals from distances 0 km

Figure 4: Distribution of Recording Stations

This figure shows the distribution of recording stations used during blast and microearthquake monitoring. The crosses denote the locations of portable stations and the triangles the location of permanent network stations. The 3 character alpha-numeric symbols are the station identifiers. The star shows the location of the blasts used to develop the velocity model.

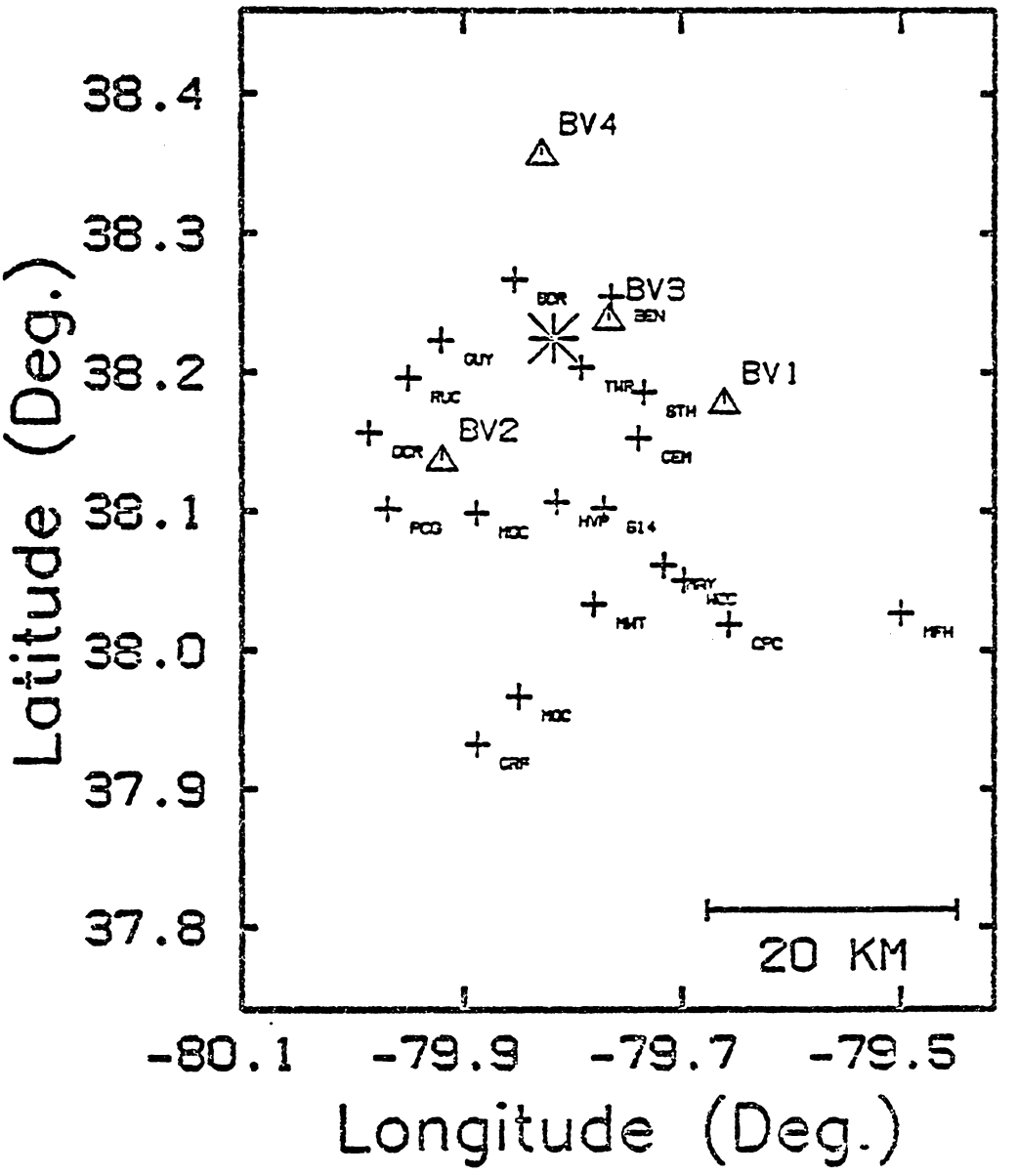
38.4
38.3
38.2
38.1
38.0
37.9
37.8
Latitude (Deg.)
-80.1
-79.9
-79.7
-79.5
Longitude (Deg.)
BV4
BV3
BV1
BV2
BEN
BDR
GUY
RUC
TMR
STH
DCR
CEM
PCG
HDC
HVP
614
HMT
CPC
HFH
HDC
CRF
20 KM

to 20 km appear to be associated with a single layer. The individual arrival-times and not the mean values are utilized in the above analyses. These data were statistically analyzed for straight line slope, intercept and velocity and intercept uncertainty after Steinhart and Meyer (1961). This yielded an upper-layer with P velocity of 5.450.09 km/sec for n=75, S velocity of 3.090.10 km/sec for n=38, and an upper-layer thickness of 3.0 km. The layer thickness was calculated by both the intercept and crossover methods (Dobrin, 1976). The values obtained by the two methods are 3.0 and 3.1 km respectively. The 3.0 km value was assumed. All uncertainties cited above and throughout this paper are for 90% confidence intervals.

The P-wave reduced travel-time curve using the true P velocity (Figure 8) shows travel- time residuals with standard deviation 0.1 seconds and distributed uniformly about zero. The S-wave reduced travel-time plot (Figure 9) shows travel-time residuals with standard deviation of 0.23 seconds and a reasonably symmetrical distribution about zero. The larger error for S is expected because it is a secondary phase.

Analyzing the most distant 2 station arrivals by the same statistical method yields a P-wave velocity of 6.041.71 km/sec for n=5. The uncertainty of this velocity is expectedly large due to the 2 stations being close together (3 km separation). However, the standard deviation of the travel-time residuals is only 0.08 seconds and the correlation coefficient is 0.95. A 6.05 km/sec layer was observed in Central Virginia

Figure 5: Mean Travel-Time vs. Distance

Plot showing P and S mean travel-times vs. distance from 0 to 40 km. The open circles denote mean P travel-times and the open triangles mean S travel-times.

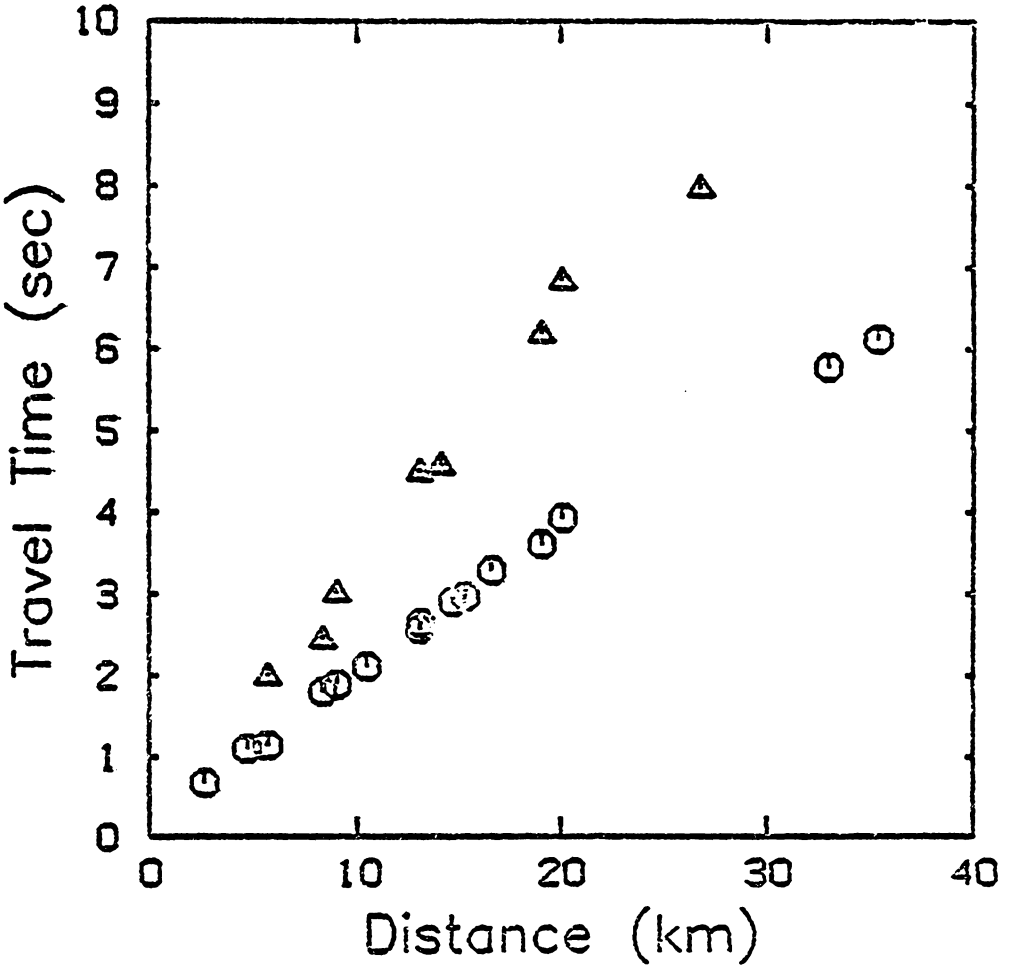
Travel Time (sec)
Distance (km)
0
1
2
3
4
5
6
7
8
9
10
0
10
20
30
40

Figure 6: Reduced P Travel-Times for Reducing Velocity 5.00 km/sec

Plot of reduced mean P travel-times (in seconds) vs. distance from 0 to 40 km. The reducing velocity is 5.00 km/sec and the reducing intercept is 0.0 sec. The reducing formula used was reduced travel time equals TT - distance/5.00.

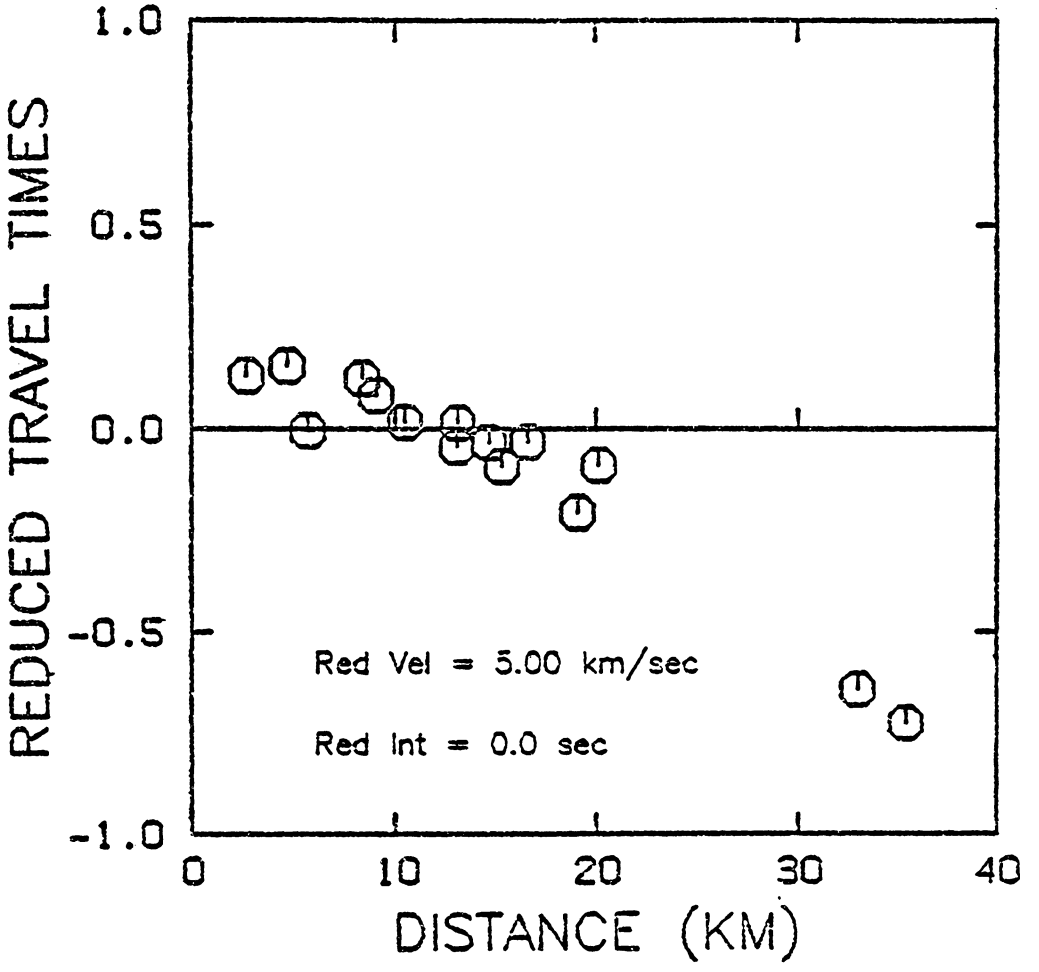
1.0
0.5
0.0
-0.5
-1.0
REDUCED TRAVEL TIMES
Red Vel = 5.00 km/sec
Red Int = 0.0 sec
0
10
20
30
40
DISTANCE (KM)

Figure 7: Reduced P Travel-Times for Reducing Velocity 6.00 km/sec

Plot of reduced mean P travel-times (in seconds) vs. distance from 0 to 40 km. The reducing velocity is 6.00 km/sec and the reducing intercept is 0.0 sec. The reducing formula used was reduced travel time equals tt - distance/6.00.

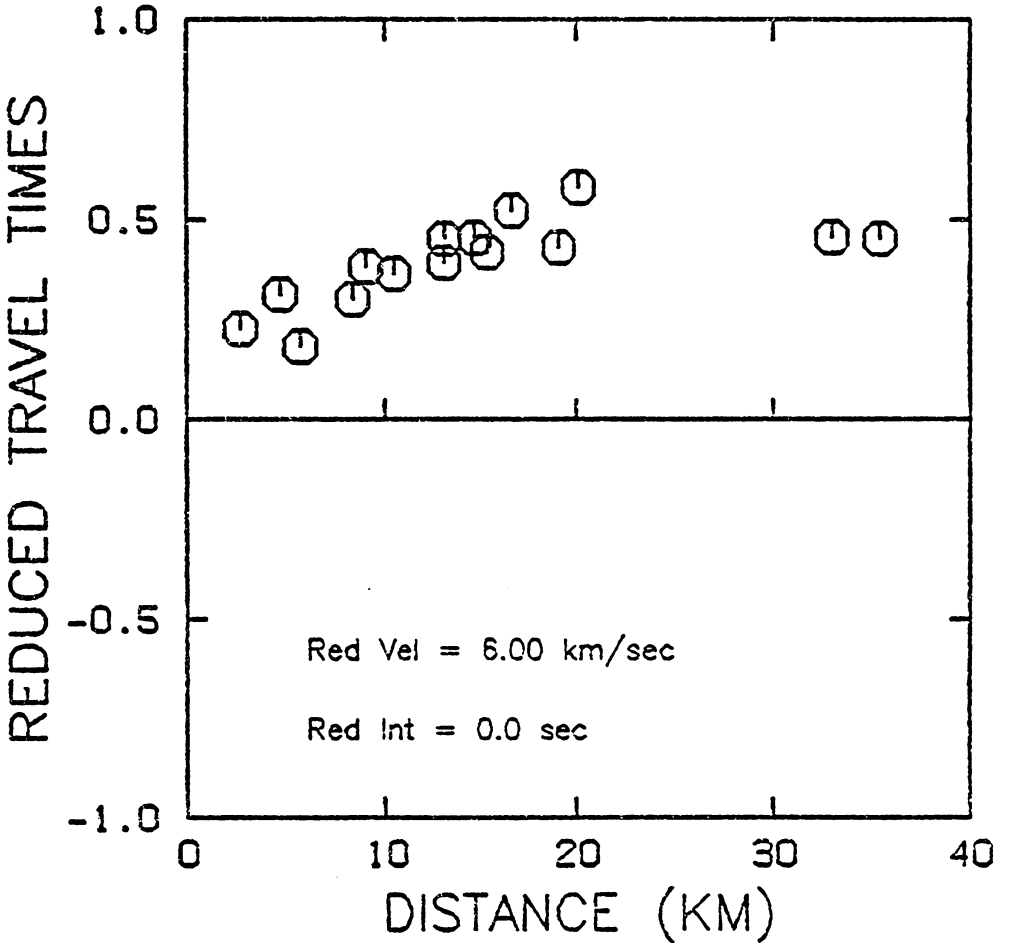
1.0
0.5
0.0
-0.5
-1.0
REDUCED TRAVEL TIMES
Red Vel = 6.00 km/sec
Red Int = 0.0 sec
0
10
20
30
40
DISTANCE (KM)

Figure 8: Reduced P Travel-Time using Measured P Velocity

Plot of reduced P travel-time (in seconds) vs. distance from 0 to 25 km. All of the reduced P travel-times are plotted as open circles. The reduced mean travel times are plotted as solid dots. The reducing velocity (5.45 km/sec) and intercept (0.16 sec) are those calculated from the leastsquares fit of the data. The reducing formula used was reduced travel time = TT - distance/5.45 + 0.16.

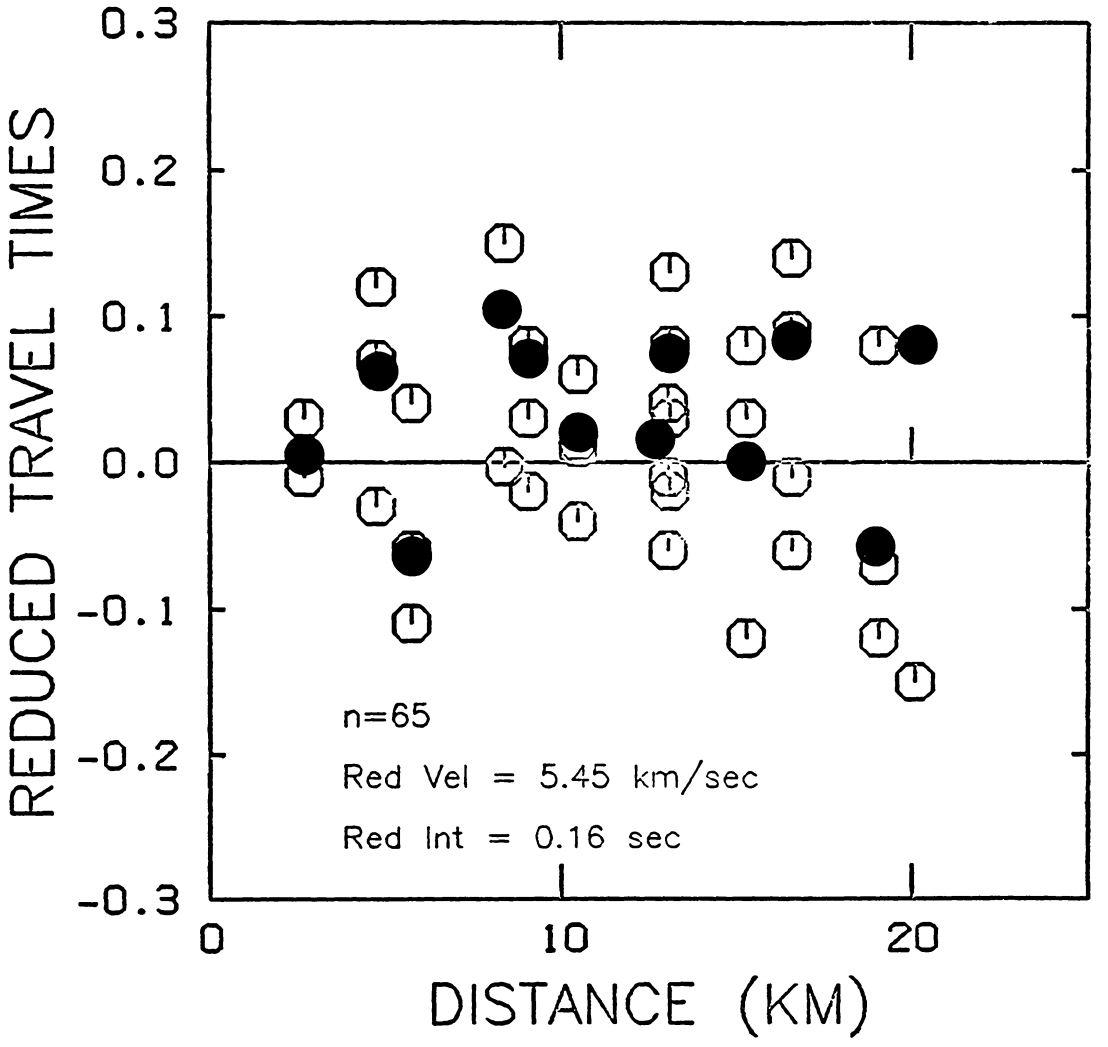
0.3
0.2
0.1
0.0
-0.1
-0.2
-0.3
REDUCED TRAVEL TIMES
0
10
20
DISTANCE (KM)
n=65
Red Vel = 5.45 km/sec
Red Int = 0.16 sec

Figure 9: Reduced S Travel-Time using Measured S Velocity

Plot of reduced S travel-time (in seconds) vs. distance from 0 to 30 km using calculated S velocity (3.07 km/sec) and intercept (-0.02 sec). All of the reduced S travel times are plotted as open circles. The reduced mean travel times are plotted as solid dots. The reducing formula used was reduced travel time = TT - distance/3.07 + -0.02.

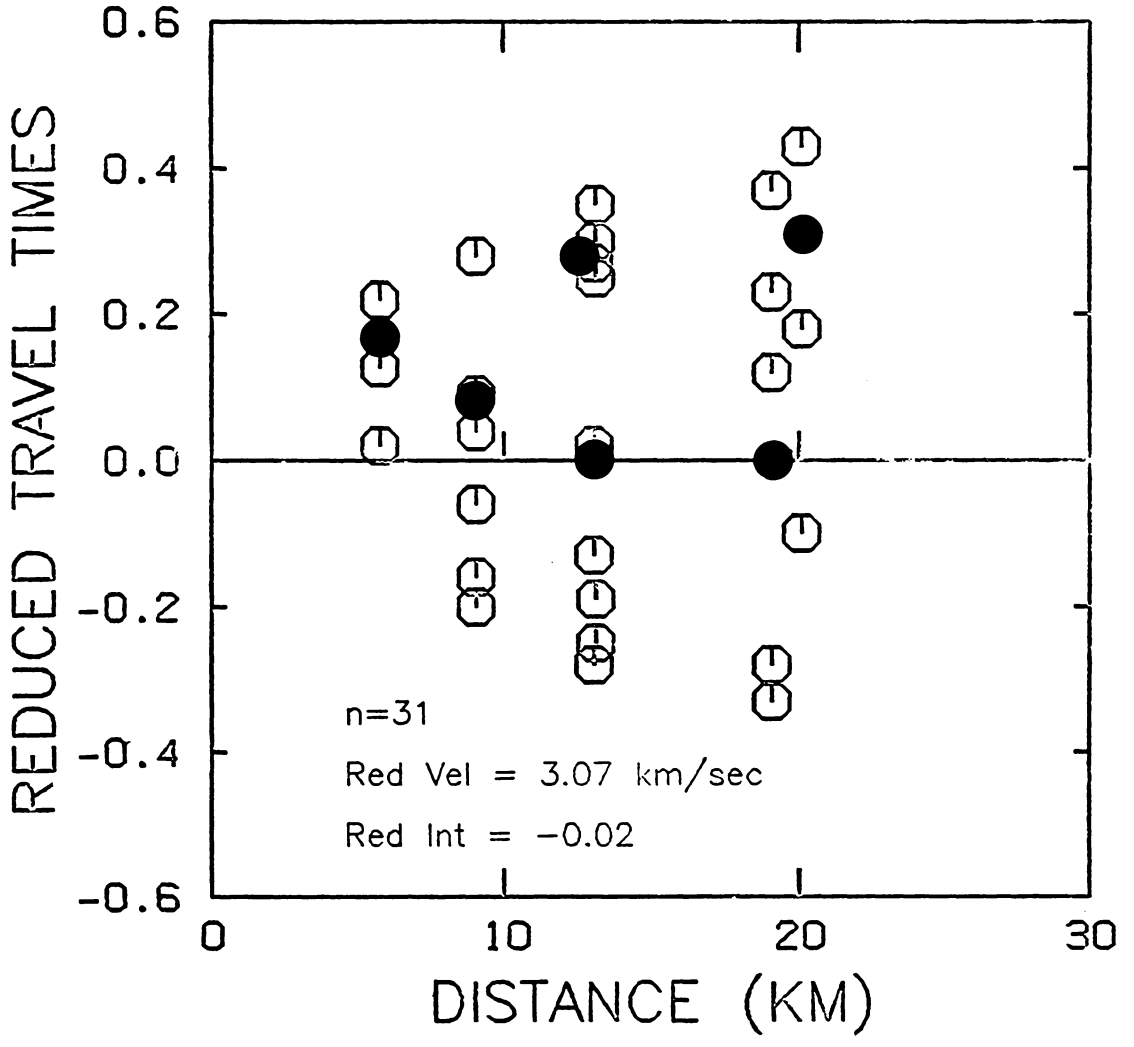
0.6
0.4
0.2
0.0
-0.2
-0.4
-0.6
REDUCED TRAVEL TIMES
0
10
20
30
DISTANCE (KM)
n=31
Red Vel = 3.07 km/sec
Red Int = −0.02

(Chapman, 1980) and was assumed in Southwest Virginia (Moore, 1980). Both velocity models have subsequently been used with good results. For uniformity, 6.05 km/sec velocity will be assumed for the second layer in Bath County.

A direct observation of the lower crustal velocity was not possible because signal attenuation precluded recording the blasts at distances greater than 35 km. Therefore, some method of estimating the lower crustal and upper mantle velocity is needed. In a study in Southwest Virginia, Moore (1980) used Tripartite Analysis to estimate the lower crust velocity. That study was also in the Valley and Ridge Province of Virginia and is only 100 km along strike to the southwest of the study area. For those reasons, the value obtained there for the velocities of the lower crust will be assumed for the Bath County area. Those P and S velocities are 6.530.22 km/sec and 3.840.08 km/sec. In the same study, Moore calculated upper mantle Pn and Sn velocities of 8.180.11 km/sec and 4.790.15 respectively. That Pn velocity agrees well with the average Southeast United States value found by Carts (1980) of 8.110.19 km/sec. Moore estimated a crustal thickness of 51 km in the Southwest Virginia area. This is similar to the value of 55 km for the Bath County area (James et al., 1968). Therefore, the values of velocities and depths for the lower two layers of the southwest Virginia model will also be assumed to be representative of the Bath County area. This composite velocity model is given in Table 1

TABLE 1

Bath County Crustal Velocity Model

P-Velocity (km/sec)	S-Velocity (km/sec)	VP/VS	Depth (km)	Thickness (km)
5.45	3.07	1.77	0.0	3.0
6.05	3.52	1.72	3.0	11.7
6.53	3.84	1.70	14.7	36.0
8.18	4.79	1.71	50.7	

2.3 GEOLOGIC INTERPRETATION OF THE DISCRETE LAYER MODEL

The upper 3.0 km of rock in the Bath County study area has a P velocity of 5.45 km/sec. This velocity is between the typical values for clastic and carbonate sediments (Dobrin, 1976). As previously mentioned, in the course of modeling the gravity anomalies in the Warm Springs area of Bath County, Kulander and Dean (1978) developed a structural model modified after Butts (1933). In their model, 3.0 km depth is near the bottom of the Cambrian-Ordovician carbonate sequence. Thus, the 5.45 km/sec velocities are probably due to the clastic and carbonate sediments of Upper Cambrian through Devonian age. The 6.05 km/sec layer, of regional extent (Chapman, 1980; Borcherdt and Roller, 1966; Dorman, 1972), represents the velocity of the Lower Cambrian and uppermost Precambrian crystalline/metamorphic layers. The lower crustal 6.53 km/sec layer continues from 14.7 km to the Moho at 51 km where the uppermost mantle P velocity is 8.18 km/sec.

The velocity studies in Southwest Virginia by Moore are close enough to the Bath County study area to compare the upper layer details of the different models. The Moore model has a top layer with P velocity 5.63 km/sec, only 3% higher than the Bath County Model. The 90% confidence intervals of the velocities overlap, implying no real statistical difference between them.

The Moore model does have one major feature not observed in the Bath County area. In the Southwest Virginia area, a velocity anisotro-

py in the upper crust was measured with the P velocity parallel to the upper crustal structure being 10% faster than the P velocity perpendicular to the structure. To test for a similar characteristic in Bath County, the data were divided into the appropriate 2 sets: parallel to the local structure (ray paths within 45 degrees of regional strike) and perpendicular to the local structure (ray paths more than 45 degrees to regional strike). These data sets were analyzed by the same statistical method as the complete data set. The P velocities were 5.41.12 km/sec and 5.350.06 km/sec for the parallel and perpendicular ray paths respectively. On the basis of the same Analysis of Variance test Moore used to confirm the velocity anisotropy, it is found that there is no velocity anisotropy in Bath County to the 99% confidence level.

The question raised by this is how a major velocity feature in Southwest Virginia could die out only 100 km to the northeast along strike. The answer may lay in the fact that the Moore model was developed in the Southern Appalachians and Bath County is in the Central Appalachians. The differing tectonic style in the Central Appalachians, absence of large scale thrusting and structures that tend to be undetached (Lowry, 1973), may affect the physical characteristics of the rocks. Also, the Southwest Virginia area is seismically active whereas Bath County has been historically aseismic. Repeated fault movements there during geologic time may have caused enough fracturing to account for the observed velocity anisotropy.

2.4 VELOCITY-GRADIENT MODELS

The observed travel-times are few enough in number and distance coverage that they can equally well result from a linear velocity gradient as from discrete velocity layers. Two velocity gradient models were analyzed. One model is a linear increase in P velocity from 5.45 km/sec at the surface to 6.53 km/sec at 50.7 km depth. This model yields a linear increase in velocity of 0.022 km/sec/km. The S velocities equal the P velocities divided by 1.74. The second model is a linear increase in P velocity from 5.45 km/sec at the surface to 6.05 km/sec at 14.7 km depth. The S velocities again equal the P velocities divided by 1.74. This model has a linear increase in velocity with depth of 0.041 km/sec/km. Below this layer is the same constant 6.53 km/sec layer as assumed in the discrete layer model. The assumed mantle velocity is 8.18 km/sec for both gradient models. When plotting the theoretical travel-time curves for these two models with the mean travel-times observed, it is apparent that both of these models are valid representations of the observed travel-times (Figure 10).

2.5 SUMMARY

Given the data set of 80 P-wave arrival-times and 38 S-wave arrival-times, the crustal velocity in the Bath County Network locale can be represented by three different models. The first model consists of 3 discrete velocity layers over the mantle. The P and S velocities of the first layer are 5.45 and 3.07 km/sec. The first layer is 3.0 km thick

Figure 10: Theoretical Travel-Time Curves for Gradient Models and Observed Mean Travel-Times

Plot of observed mean P-wave travel-times (open circles) vs. distance superimposed on the theoretical travel-time curve for Model 2 from 0 to 40 km. The theoretical travel time curves for Model 2 and Model 3 are virtually identical, so only Model 2 is plotted here.

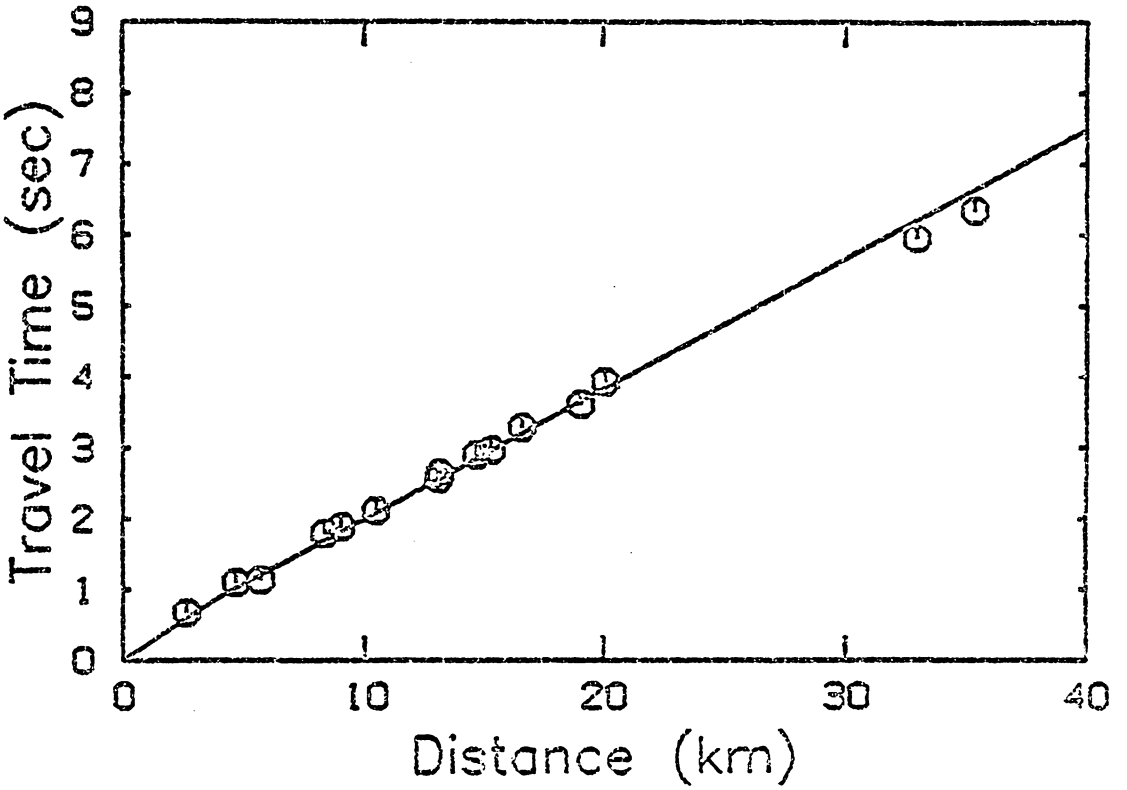
Travel Time (sec)
0
1
2
3
4
5
6
7
8
9
0
10
20
30
40
Distance (km)

and represents the velocity of Upper Cambrian through Devonian sediments. The second layer has P and S velocities 6.05 and 3.52 and is 11.7 km thick. This layer represents the Lower Cambrian sediments and the crystalline upper basement rocks. The third layer has P and S velocity 6.53 and 3.84 km/sec and is 36 km thick. The uppermost mantle has P and S velocities of 8.18 and 4.79 km/sec. This will later be referred to as Model 1. Another possible model is a linear increase in P and S velocity from (respectively) 5.45 km/sec and 3.07 km/sec at the surface to 6.53 km/sec and 3.84 km/sec at 50.7 km depth. Beneath this layer is the mantle with P and S velocities 8.18 km/sec and 4.79 km/sec. This will be referred to as Model 2. The final possible model considered uses a linear increase in P and S velocity from 5.45 km/sec and 3.07 km/sec at the surface to 6.05 km/sec and 3.52 km/sec at 14.7 km depth. The remainder of the model is the same as the discrete velocity layer model. This model will be referred to as Model 3. Figure 11 shows the plot of the three velocity models as a function of depth. These three models cannot be distinguished on the basis of the travel-times recorded in this study. No azimuthally dependent velocity anisotropy was observed.

A version of Model 1 with a low-velocity surficial layer was briefly considered. This model eliminates the disparity between the 0.16 sec intercept time of the P travel-time curve and the expected value of 0.0 sec. This model will be tested and discussed in a later section.

Figure 11: Plot of the 3 Crustal and Upper Mantle Velocity Models as a Function of Depth

Plot of Velocity vs. Depth for the 3 Bath County velocity models being considered. The solid line is the discrete velocity layer model (Model 1). The line with short dashes is Model 2 and the line with long dashes is Model 3. The two dashed lines meet with the solid line at the depths for which the model velocities converge.

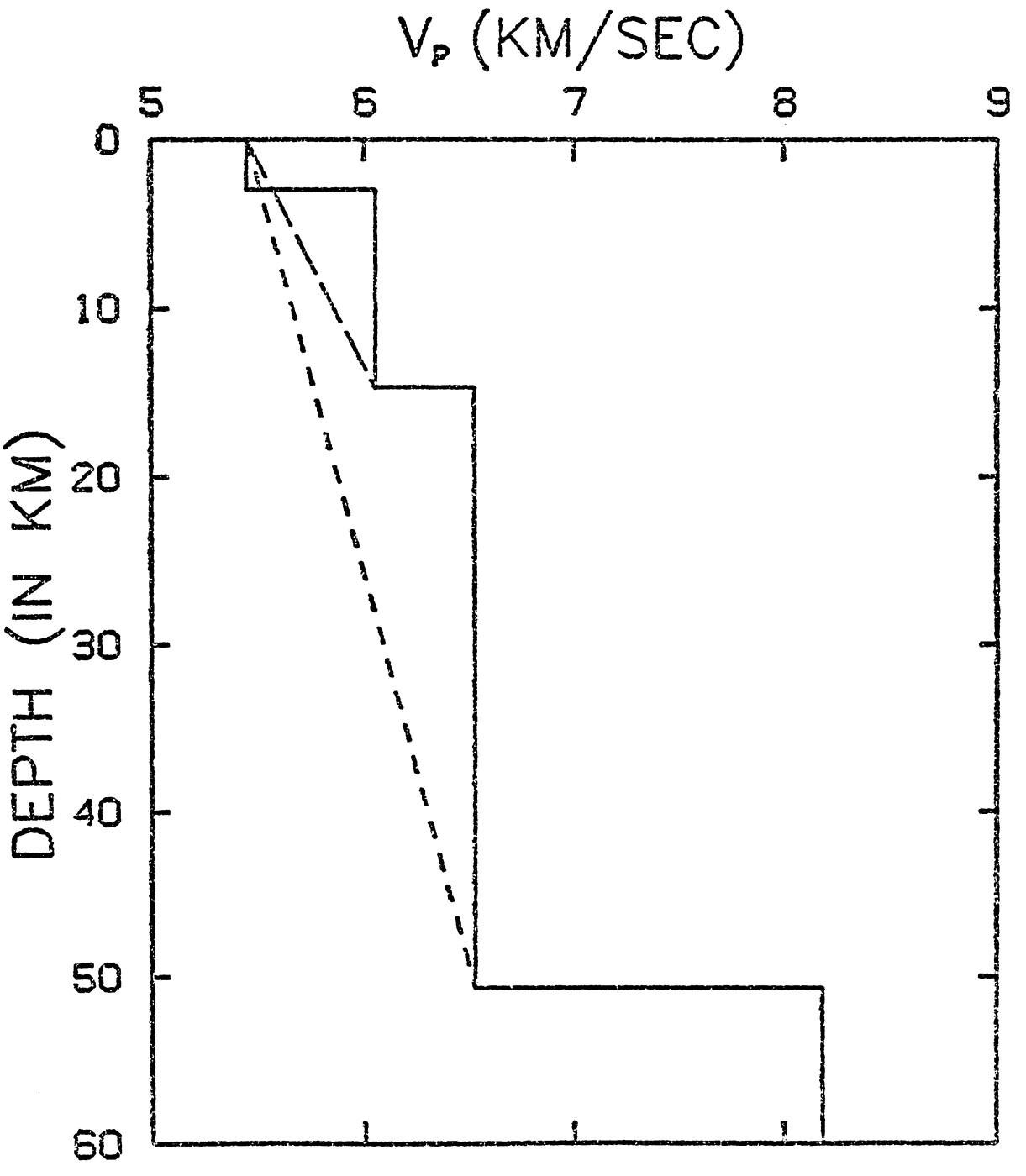
V_P (KM/SEC)
5
6
7
8
9
0
10
20
30
40
50
60
DEPTH (IN KM)

Chapter III

TESTING THE BATH COUNTY NETWORK VELOCITY MODEL

A test of the locational capability of the Bath County Seismic network was conducted using the aforementioned velocity models. The test consisted of locating quarry and construction blasts in the study area and comparing their actual locations with the calculated locations derived from HYPOELLIPSE (Lahr, 1980). The adequacy of the HYPOELLIPSE locations were judged by three criteria: the average epicentral distance from the center of the error ellipse to the actual blast location, the number of error ellipses that enclose the blast site, and whether the calculated depths were close to zero regardless of the initial trial focal depth used.

This test was carried out for two sources. The first source was a construction blast site near the central station of the network, BV3. This is the same source from which the velocity model was derived using an origin-time seismograph and the mobile/fixed networks. Thus, using this source does not constitute an independent test of the locational capability of the network and model. However, this source is well inside the permanent network and since a separate set of blasts were used, should give an adequate test of locational capability. The GAP (largest epicenter-to-station azimuthal angle with no station coverage) for this source is 135 degrees. The second source was a stone quarry on the edge of the network with a GAP of near 180 degrees.

Figure 12 shows the locations of these two sources in relation to the network stations.

3.1 LOCATIONAL CAPABILITY INSIDE THE NETWORK

Five blasts from a construction area on the Vepco project site were located using arrival-time data from the permanent network stations and velocity Model 1. Each blast generated P and S phases to all four network stations. Table 2 gives the epicentral distance and azimuth from the actual blast location to the HYPOELLIPSE location. The average locational error (delta) is 0.6 km which is excellent. Figure 13 shows the blast locations and the error ellipses calculated by HYPOELLIPSE in relation to the blast site. Notice that all of the error ellipses enclose the blast site. The small locational errors and the enclosing of the blast site by the error ellipses together imply good epicentral control for this source.

The other important location parameter to be tested is the focal depth. Because all of these blasts were at the surface, HYPOELLIPSE should, in principle, return solutions with zero depths regardless of the trial focal depths used. If the depth of the solution changes radically with the different trial focal depths, then the locations have poor vertical control. However, if the depths converge towards the surface for differing trial focal depths, then the depth is probably at a global and not a local minimum.

Figure 12: Location of Blast Sources

Location of quarries used in the location tests in relation to the Bath County Seismic Network. The source quarries are denoted by stars and the network stations by open triangles with 3 character alpha-numeric codes.

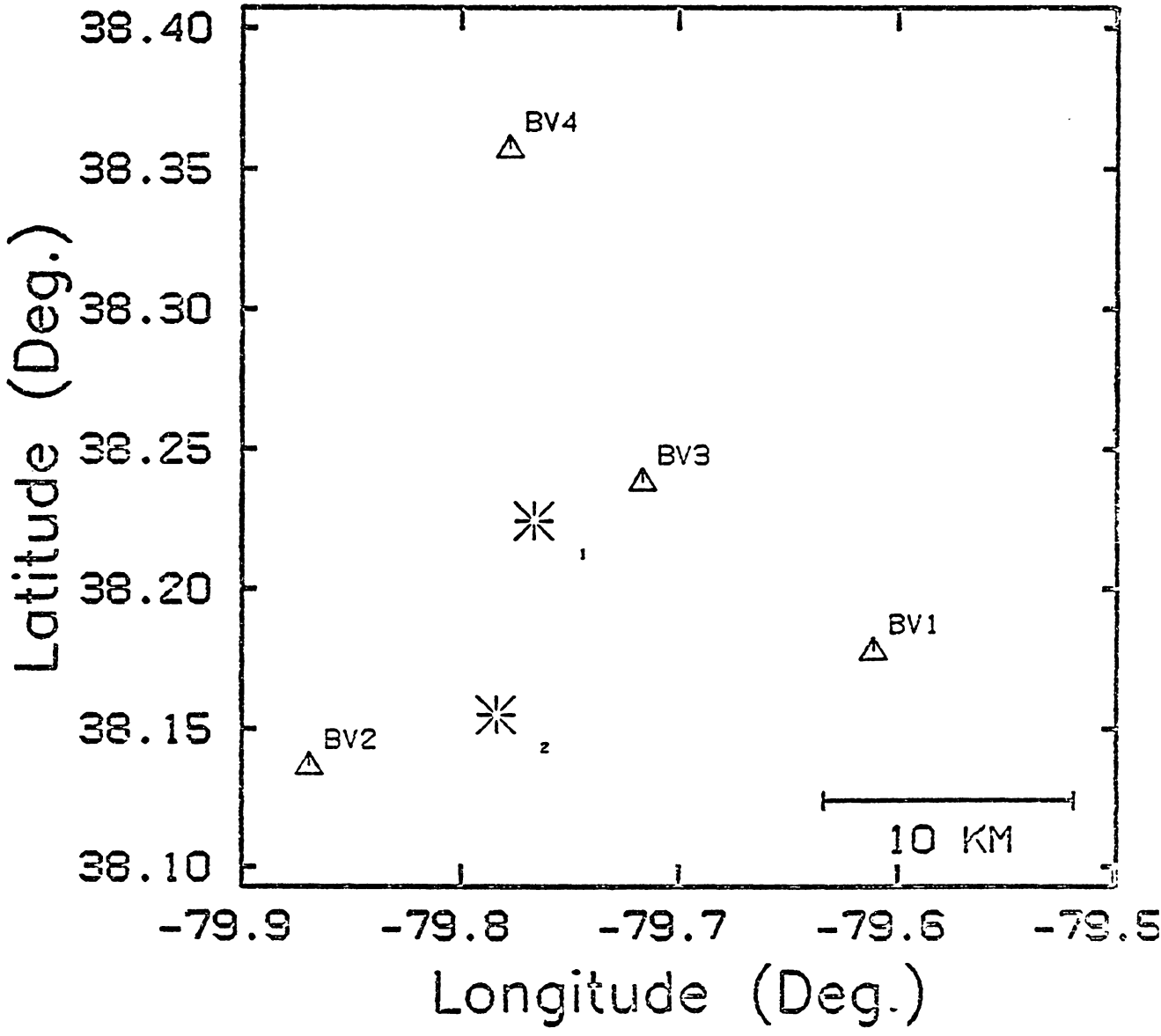
38.40
38.35
38.30
38.25
38.20
38.15
38.10
Latitude (Deg.)
BV4
BV3
BV1
BV2
1
2
10 KM
-79.9
-79.8
-79.7
-79.6
-79.5
Longitude (Deg.)

Figure 13: Locations and Error Ellipses for Model 1 Locations Inside the Network

Hypoellipse locations and error ellipses for blasts originating inside the network located by Model 1. The star is the blast source and the small open circles are the calculated epicenters. The ellipses are the horizontal projections of the HYPOELLIPSE error ellipsoids.

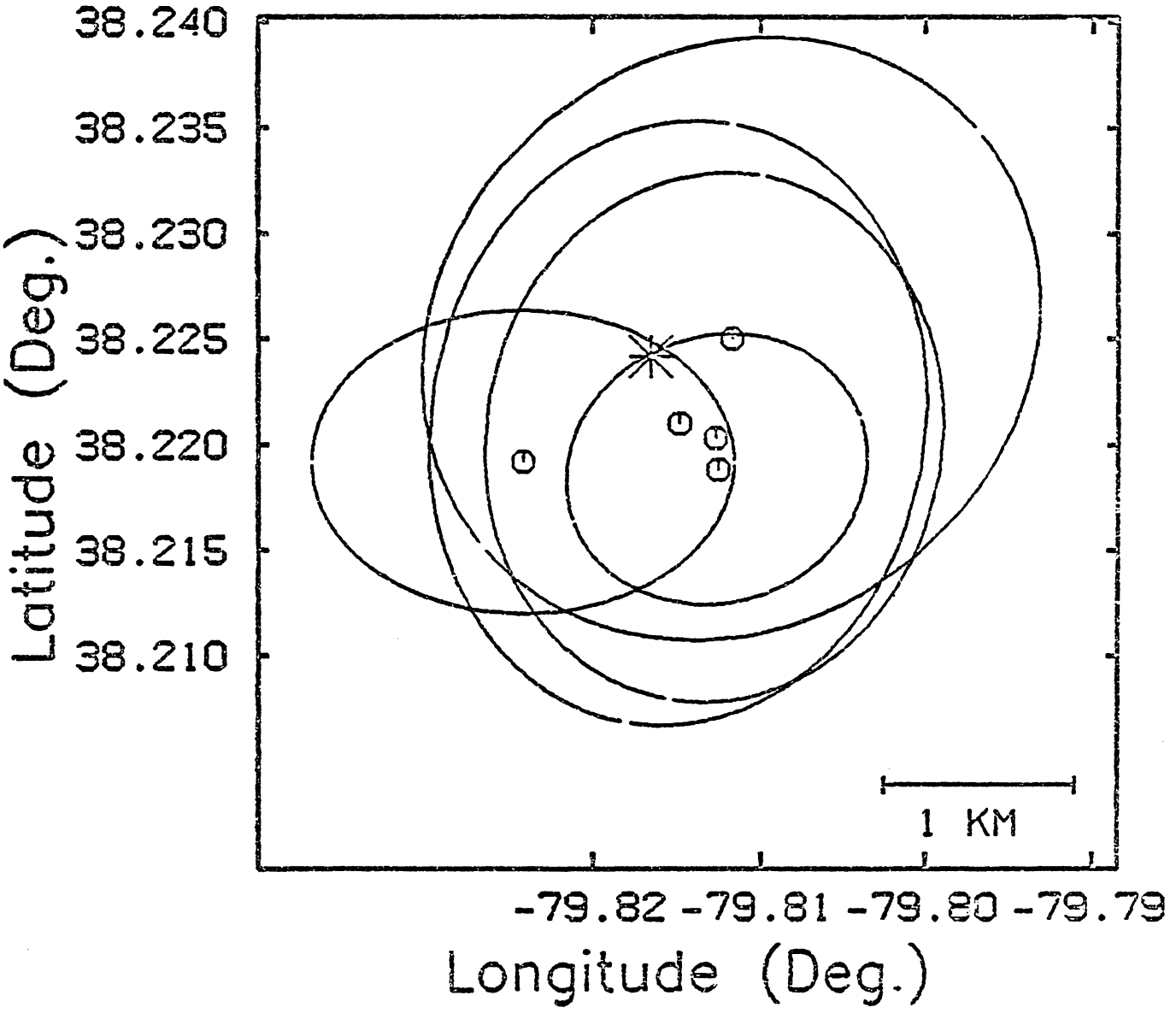
38.240
38.235
38.230
38.225
38.220
38.215
38.210
Latitude (Deg.)
1 KM
-79.82 -79.81 -79.80 -79.79
Longitude (Deg.)

The depths and vertical confidence regions for the five blasts using Model 1 are presented in Table 3 The solutions were started at depths of 1.5, 5.0, 10.0, and 20.0 km. The ERZ shown in the table is the vertical projection of the HYPOELLIPSE calculated error ellipsoid. The large values for ERZ are due primarily to the fact that there is no station within a horizontal distance equal to the focal depth. For these blasts with a focal depth of zero, this would require an origin-time geophone. Notice that all of the depths are within 3.0 km of the surface and that there is no relation between trial focal depth and final depth. Finally, note that vertical error ellipse encloses the surface in all cases. Collectively, these results imply good vertical control. Table 4 lists the detailed locational criteria for the five blasts using 10 km as the trial focal depth.

TABLE 2

Epicentral Errors at Quarry One for Model 1

Quarry Location Lat. 38N13.45 Lon. 79W48.99

Date (Yr/Mo/Day)	Delta[1] (km)	Azimuth (Deg)
820727	0.39	203
820728	0.55	217
820729	0.87	129
820729	0.43	281
820730	0.70	210
AVERAGE	0.59	208

[1]Difference between actual and calculated location.

TABLE 3

Depths and Vertical Errors for Different Trial Focal Depths (TFD) from Model 1 at Quarry One

TFD	Blast 1 DepthERZ	Blast 2 DEPTHERZ	Blast 3 DEPTHERZ	Blast 4 DEPTHERZ	Blast 5 DEPTHERZ
1.5	0.264.7	0.434.4	0.621.6	0.199.0	0.88.9
5.0	0.199.0	0.435.4	0.524.6	2.82.9	0.98.0
10.0	0.265.6	0.430.3	0.524.9	0.362.7	0.88.9
20.0	0.434.7	0.619.9	0.430.1	0.099.0	0.79.9
Ave	0.2366.0	0.4530.0	0.525.3	0.865.9	0.88.9

TABLE 4

Locational Criteria for Quarry One Locations

Date	No of Phases (P/S)	RMS Res (sec)	ERH (km)	DMIN (km)	GAP (deg)	Ellipse Quality	Solution Quality
820727	4/4	0.21	1.6	4.6	131	D	C/B
820728	4/4	0.18	1.4	4.5	130	D	C/B
820729	4/4	0.14	1.1	5.5	136	D	C/C
820730	4/4	0.24	1.7	4.2	131	D	C/B
820730	4/4	0.13	0.8	4.6	129	C	C/B
AVE	4/4	0.18	1.3	4.7	131	D	C/B

Criteria derived from HYPOELLIPSE(Lahr, 1980).

3.2 LOCATIONAL CAPABILITY ON THE EDGE OF THE NETWORK

The second source used to test the locational capability of the Bath County Network was a stone quarry on the edge of the network (Figure 12). Each of five blasts were recorded on all four of the Bath County stations and were located using at least 7 P and S phases. The distances and azimuths from the blast site to the HYPOELLIPSE locations are given in Table 5. The average mislocation (delta) for this quarry is 2.0 km. This is three times that for the previous source and, because this quarry is on the edge of the network (GAP = 180), is expectable.

Figure 14 shows the HYPOELLIPSE locations and error ellipses for these 5 blasts in relation to the quarry location. Note that only 2 of the 5 (40%) of the error ellipses enclose the blast site. The larger delta and the fewer enclosures of the blast site by the error ellipses document the poorer epicentral control for sources at the edge of the network.

The depth control test was also performed for these five locations by employing different trial focal depths (1.5, 5.0, 10.0 and 20.0 km). The final depths computed and ERZs are listed in Table 6 Notice that the final depths are both greater and less than one confidence interval from the surface and that the final depths do not vary greatly with varying trial focal depth. Also, the depth variations from blast to blast as well as the failure of some confidence intervals to include the surface, indicates poor vertical control. The error criteria resulting from the 10 km trial focal depth locations are given in Table 7.

Figure 14: Locations and Error Ellipses for Model 1 Locations Outiside the Network

HYPOELLIPSE locations and error ellipses for blasts originating on the edge of the network as located by Model 1. The star is the location of the blasts and the small open circles the calculated epicenters. The ellipses are the horizontal projection of the HYPOELLIPSE error ellipsoids.

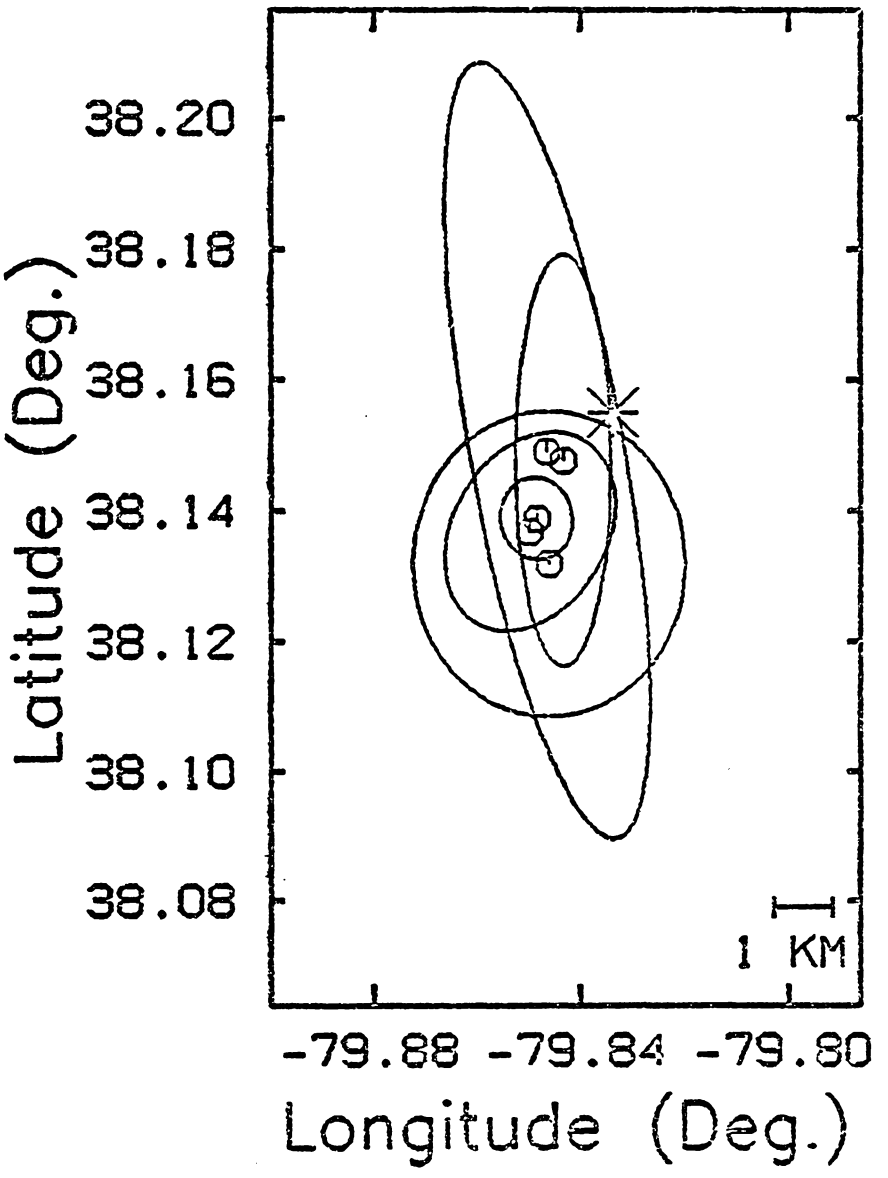
38.20
38.18
38.16
38.14
38.12
38.10
38.08
Latitude (Deg.)
1 KM
-79.88 -79.84 -79.80
Longitude (Deg.)

TABLE 5

Epicentral Errors at Quarry Two for Model 1

Quarry Location Lat. 38N09.30 Lon. 79W50.02

Date (YrMoDay)	Delta[1] (km)	Azimuth (deg)
810521	1.00	127
810624	2.46	145
810715	2.21	144
811216	2.79	157
820106	1.29	121
AVERAGE	1.95	139

[1]Difference between actual and calculated locations.

TABLE 6

Depths and Vertical Errors for Different Trial Focal Depths (TFD) from Model 1 at Quarry Two

TFD	Blast 1 Depth	ERZ	Blast 2 Depth	ERZ	Blast 3 Depth	ERZ	Blast 4 Depth	ERZ	Blast 5 Depth	ERZ
1.5	0.1	99.0	6.5	4.0	11.0	1.5	11.7	5.8	1.2	10.6
5.0	1.5	5.2	6.5	4.0	11.0	1.5	12.7	6.6	0.9	11.4
10.0	1.5	5.2	6.5	4.0	11.0	1.5	11.7	5.8	0.9	11.5
20.0	2.3	3.3	6.5	4.0	11.0	1.5	12.7	6.6	0.9	11.5
Ave	1.4	28.2	6.5	4.0	11.0	1.5	12.2	6.2	1.0	11.3

[1]TFD and ERZ from HYPOELLIPSE (Lahr, 1980).

TABLE 7

Locational Criteria for Quarry Two Locations

Date	No of Phases (P/S)	RMS Res (sec)	ERH (km)	DMIN (km)	GAP (deg)	Ellipse Quality	Solution Quality	
810521	4/3	0.11	3.4	6.8	182	C	C/D	
810624	4/4	0.14	1.8	6.1	195	B	B/D	
810715	4/3	0.04	0.7	6.2	193	A	A/D	
811216	4/3	0.17	2.6	6.5	202	C	C/D	
820105	4/3	0.18	6.7	6.6	179	D	C/C	
AVERAGE		4/3	0.13	3.0	6.4	190	C	C/D

The gradient Models 2 and 3 were also tested. One blast from each of the sources was relocated using these two models. The resulting calculated locations of these blasts were, as expected, virtually identical to the locations obtained using the discrete layer model discussed earlier.

The same tests were repeated for an additional velocity model with a a low velocity layer (5.0 km/sec, 2.3 km thickness) at the surface. Such a surficial layer is geologically reasonable and would eliminate the disparity between the observed intercept time of 0.16 sec and the expected intercept time of 0.0 sec. The epicentral errors resulting from the use of this model remained nearly the same (<1 km inside the network, 3.0 km on the edge of the network) but the depth control degraded somewhat (depths averaged 2.0 km inside the network and varied greatly on the edge of the network). Because of the poorer depth control, this model is not considered further.

In summary, the location tests have demonstrated two principal factors. First, the discrete velocity layer model and the gradient models can produce accurate locations for sources inside the network. There was less than 1 km of epicentral error inside of the network and all of the error ellipses enclosed the actual location. The depth control was also good. The locations averaged less than 1 km depth and all of the confidence regions enclosed the surface. Second, the locational accuracy degrades quickly for sources outside of the network for all three models. On the edge of the network, there is 3 km of epicentral error and depth control is absent.

Chapter IV

SEISMICITY OF THE BATH COUNTY AREA

The record of seismicity in Bath County is derived from four sources: (1) the historical (pre-instrumental) period, (2) a microearthquake reconnaissance study in 1973 (Bollinger and Gilbert, 1974), (3) a 47 day field monitoring program (this study, June-August, 1982), and (4) the network monitoring results from November 1978 to November 1982.

Historically, the study area shows no felt seismic activity (Bollinger, 1975). That is, there is no record of earthquakes originating in the area large enough to be felt by humans. The study area is a quiescent zone contained in the relatively active zone of the host Appalachians. To the southeast in the Piedmont province, the Central Virginia area has also been active (Figure 15).

A short-term microearthquake monitoring effort was carried out in June, 1973 (Bollinger and Gilbert, 1974). During that study, 438 hours of low noise data were collected at 7 sites in Bath and Highland Counties, Virginia. A swarm of 43 microshocks was recorded at one of the stations. The S-P times of the events were less than 0.2 seconds, implying distances within 2 km of the station. The amplitudes of the events indicated magnitudes ranging from -1/2 to -1. Their durations of less than 3 sec implies even smaller magnitudes. Bollinger (personal communication, November 1982) suggests that these events by them-

Figure 15: Historical Epicenters in Virginia and West Virginia

Map showing the distribution of historical epicenters in Virginia and West Virginia. The dots indicate locations of historical earthquakes with the size of the dot scaled to the maximum intensity. Dots with X's in them indicate multiple epicenters. The star is located at Hot Springs, Virginia, located in Bath County. The dashed box si to draw attention to the aseismic character of the Bath County area. After Bollinger and Gilbert (1974).

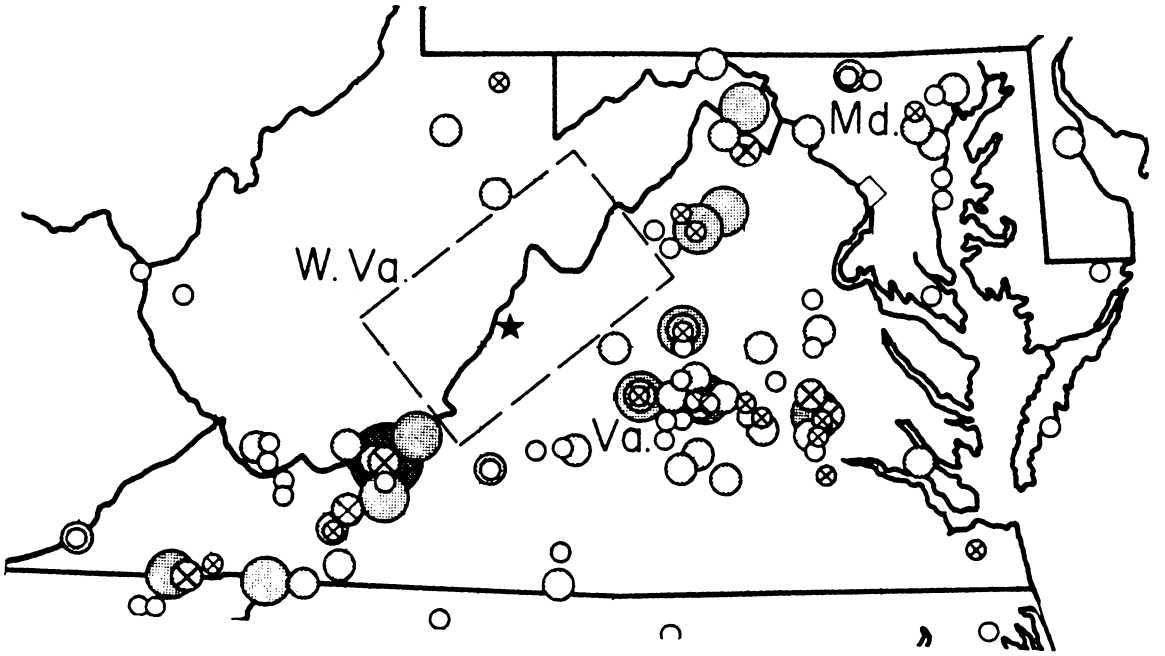
Md.
W. Va.
Va.

selves have little tectonic significance and were probably caused by surface thermal fracturing, regolith creep, perhaps aided by ground water lubrication, or other non-tectonic causes. This general lack of microseismicity agrees with the historical seismic quiescence.

During the course of blast monitoring, discussed in Chapter 2, 3,120 hours of low noise data were collected at 19 sites in Bath and Highland Counties in Virginia and Pocahontas County in West Virginia. Monitoring was conducted from June 25 until August 30. Four seismographs were used as a mobile array. The site locations are shown in Figure 4. During this monitoring time-frame, no natural seismic events were recorded, which is consistent with the historical aseismicity.

A four station microearthquake monitoring network has been operational in Bath County, Virginia since November, 1978. The network has an aperture of 25 km and a central station near the Vepco Bath County Pumped Storage Project. Since network monitoring began, 8 locatable events and 3 unlocatable events have been recorded. The 3 events were unlocatable because they were too small to be recorded at enough stations. The events range in magnitude from Md= -0.6 to mbLg= 3.0. None of the events were felt. The low frequency of the seismicity (11 events in 4 years) and the fact that none of the events were felt again supports the relatively aseismic character of the area. Table 8 gives the dates and magnitudes of the located events. Detailed information on epicenters, focal depths, solution-quality, etc. may be found in Tables 9, 10 and 11.

TABLE 8

Dates and Magnitudes of the Bath County Seismic Events

November 1978 to November 1982.

Event	Date	Magnitude
42B	Sep 16, 1979	1.6
42C	Sep 19, 1979	1.8
55A	Sep 21, 1980	1.4
61	Oct 16, 1980	0.9
61A	Nov 5, 1980	3.0
62	Nov 25, 1980	0.6
68	Apr 11, 1981	-0.6
70	Jun 6, 1981	0.7

4.1 EVENT LOCATION

Event locations were calculated by the program HYPOELLIPSE utilizing the 3 crustal velocity models discussed in Chapters 2 and 3. Eight reset variables were altered from the default values in an effort to fine tune hypocentral accuracy. These reset variables resulted in the use of elevation corrections (P-velocity of 5.45 km/sec), distance weighting to the arrival-times, deletion of arrival-times with large residuals and multiplication of S-phase arrival-time weights by 0.75.

The event locations and error statistics for the discrete layer model (Model 1) are given in Table 9. The RMS residuals average 0.20 seconds and the ellipse qualities average B. Depths range from 7.1 km to 17.4 km with ERZ's from 1.1 km to 13.5 km. Figure 16 shows the epicentral locations of the events. Notice that the events trend roughly east-west and exhibit some scatter. The 8 events span an east-west distance of 80 km with an average event spacing of 10 km. Three of the events, 42B, 42C and 61 are within 6 km of each other.

The event locations and errors using the gradient over mantle velocity model (Model 2) are given in Table 10 The average RMS residual is 0.40 sec and the average ellipse quality is C. The large average RMS and lower average ellipse quality, as compared to Model 1 results, indicate that this model was not optimum for event location. Thus, Model 2 has been eliminated as a possible representation of crustal velocity and will not be considered further.

Figure 16: Locations and Error Ellipsoid Projections of Network Recorded Events Located by Model 1

HYPOELLIPSE locations and error ellipse projections of the network recorded events located by Model 1. The open circles are the epicentral locations with the size of the circle scaled to the magnitude of the event. The bars are the horizontal projections of the calculated error ellipse axes.

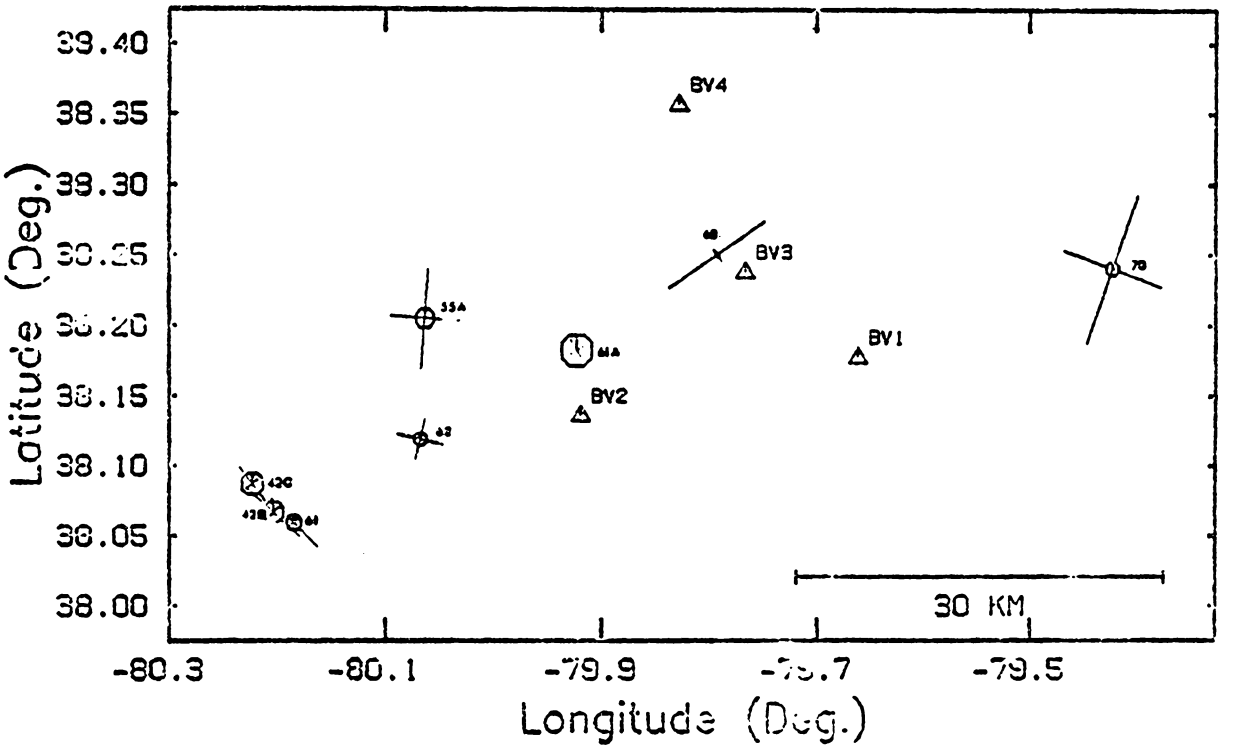
39.40
38.35
38.30
38.25
38.20
38.15
38.10
38.05
38.00
Latitude (Deg.)
-80.3
-80.1
-79.9
-79.7
-79.5
Longitude (Deg.)
BV4
BV3
BV1
BV2
30 KM

The event locations and error statistics for velocity Model 3 (gradient over layer over mantle) are given in Table 11. The average RMS residual is 0.18 sec and the average ellipse quality is B. The depths vary from 7.3 km to 17.6 km with ERZ's from 1.3 km to 19.3 km. These locations imply that this model is effectively locating the events, and therefore must be a reasonable representation of crustal velocity. The epicentral locations are shown in Figure 17. Notice that the epicenters have not changed significantly from the discrete layer model. The east-west trend of the events is still evident.

In summary, the event locations indicate an apparent linear pattern of seismicity in the Bath County area. Two crustal velocity models were shown to be adequate for locational purposes. These two are the discrete layer model and the gradient over layer over mantle model. The gradient over mantle model performed poorly and has been discarded as a possible representation of crustal velocity. As most of the events locate outside of the network, a minimum epicentral error of 3 km can be expected. Depth control should also be poor, except for events 61A, 62, and 68, which have a station at an epicentral distance less than 1 focal depth.

Figure 17: Locations and Error Ellipsoid Projections of Network Recorded Events Located by Model 3

HYPOELLIPSE locations and error ellipse projections of the network recorded events located by Model 3. The open circles are the epicentral locations with the size of the circle scaled to the magnitude of the event. The bars are the horizontal projections of the calculated error ellipse axes.

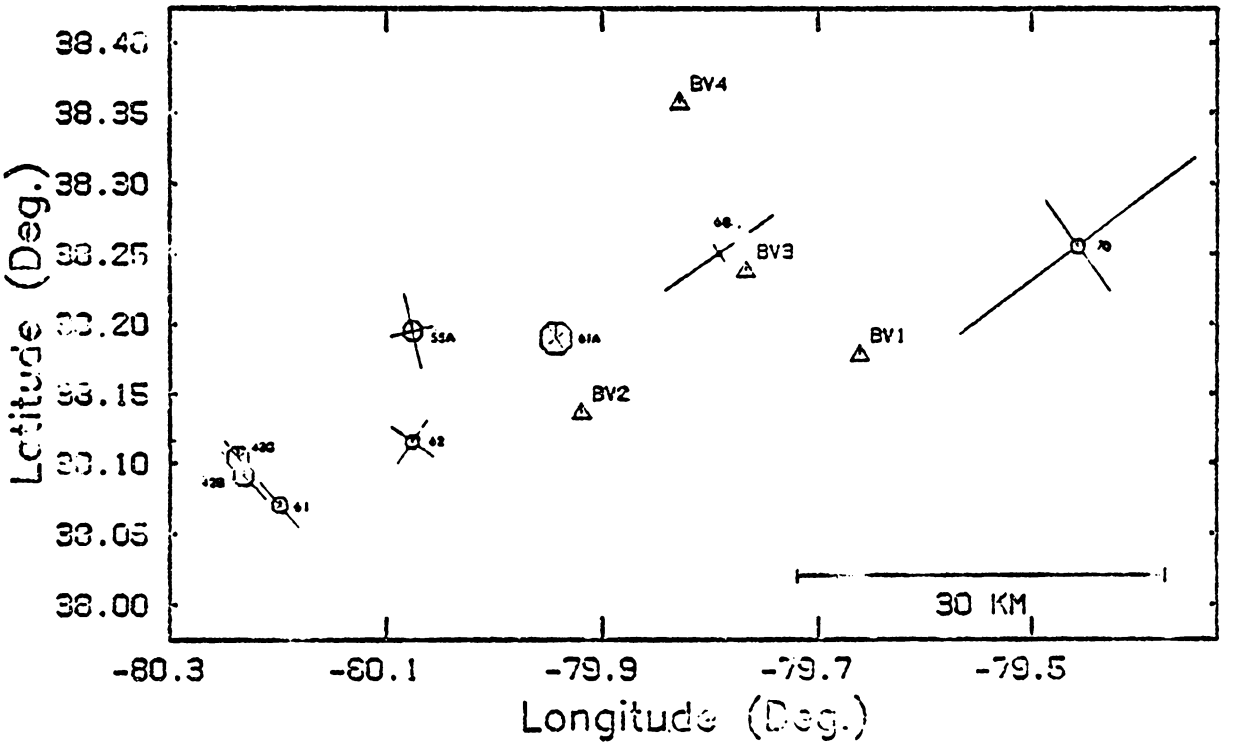
38.40
38.35
38.30
38.25
38.20
38.15
38.10
38.05
38.00
Latitude (Deg.)
-80.3
-80.1
-79.9
-79.7
-79.5
Longitude (Deg.)
BV4
BV3
BV1
BV2
30 KM

TABLE 9

Event Locations and Error Statistics for Discrete Layer Model (Model 1)

Ev	Depth	GAP (km)	RMS (sec)	ERH (km)	ERZ (km)	No of Phases	Ellipse Quality	Epicentral Quality
42B	16.7	194	0.20	2.9	5.2	13	C	C/D
42C	17.4	184	0.18	1.7	3.8	20	B	B/D
55A	11.6	198	0.22	3.9	7.3	8	C	C/D
61	15.0	175	0.19	2.7	4.8	13	B	C/C
61A	8.8	73	0.23	1.0	1.1	34	A	B/A
62	14.5	317	0.09	1.9	2.3	8	A	B/D
68	9.6	220	0.06	4.7	1.8	6	B	C/D
70	7.1	322	0.39	6.2	13.5	8	D	D/D

TABLE 10

Event Locations and Error Statistics for Gradient over Mantle Model (Model 2)

Ev	Depth	GAP (km)	RMS (sec)	ERH (km)	ERZ (km)	No of Phases	Ellipse Quality	Epicentral Quality
42B	22.5	186	0.28	4.3	2.9	13	B	C/D
42C	23.9	175	0.47	4.5	4.8	20	B	C/C
55A	23.7	197	0.46	8.9	6.4	8	C	D/D
61	16.2	172	0.31	4.2	8.4	13	C	C/C
61A	15.7	76	0.78	3.4	3.8	33	C	D/A
62	15.9	316	0.11	2.2	2.5	8	B	C/D
68	9.9	202	0.06	5.2	2.1	6	C	D/D
70	14.8	324	0.74	14.9	28.7	8	D	D/D

TABLE 11

Event Locations and Error Statistics for Gradient over Layer over Mantle Model(Model 3)

Ev	Depth	GAP (km)	RMS (sec)	ERH (km)	ERZ (km)	No of Phases	Ellipse Quality	Epicentral Quality
42B	14.6	200	0.19	2.6	2.0	13	B	C/D
42C	17.6	189	0.16	1.7	4.1	19	B	B/D
55A	7.3	197	0.17	3.0	5.3	8	C	C/D
61	13.9	179	0.16	2.4	1.7	13	A	C/C
61A	8.0	148	0.26	1.2	1.3	29	A	B/C
62	15.3	319	0.10	2.1	2.3	8	A	C/D
68	10.1	220	0.06	5.3	2.1	6	C	D/D
70	11.9	315	0.37	11.9	19.3	8	D	D/D

4.2 FOCAL MECHANISM STUDY

To better understand the stress regime responsible for the activity in the Bath County Area, a focal mechanism study was conducted for the events. P-wave polarities and SV/P amplitude ratios were used to define valid sets of B, P and T axes (Tzeng, 1982). This technique was used for single events and for composites of events. The polarity and amplitude ratio data were analyzed for velocity Models 1 and 3.

The method used is an iterative search by computer over the focal sphere for possible sets of B,P and T axes. The inputs to the program are the P-wave polarities, the SV/P amplitude ratios (after being corrected for the free surface effect), the epicenter-to-station azimuths and the angles of incidence at the source. The program tests for agreement between the input data and values it calculates for an extensive sample of possible values of B, P and T axes. The degree of agreement between the input and calculated values is also specified as an input.

This method introduces several asumptions into the data analysis that are worth noting specifically. Those assumptions are:

1. The calculated take-off angle at the earthquake source is accurate. Since the SV/P amplitude ratio varies non-linearly over the focal sphere, the estimate of the P and SV take-off angles must be accurate to obtain a reliable focal mechanism.
2. The angle of emergence at the surface is well known. This is important because the free surface effect on the SV/P amplitude

ratio must be calculated. This method assumes that the take-off angle and the angle of emergence at the surface are exactly the same.

3. The P and SV waves have identical take-off angles and travel paths to the recording station. This condition, in turn, assumes the following:
   a) The Poisson's ratio does not change vertically or horizontally.
   b) The crustal velocity does not change horizontally.
4. Q is very similar for P and SV. The amplitude of both P and SV must be attenuated by the same percentage for the amplitude ratio to be valid. Thus, if the travel paths are not the same, then the anelasticity will not affect P and SV the same.

The effect of these assumptions on the reliability of focal mechanisms calculated by this method is worthy of further investigation. Some of these asssumptions are clearly violated to some degree when working with actual earthquake data. However, for the purposes of this study, it will be assumed that the above assumptions have been met well enough that a reasonably reliable focal mechanism can be obtained.

To assure the best possible results, only those events with the most reliable hypocentral locations were used. Here, reliable is taken to mean locations with A and B quality ellipses (events 42B, 42C, 61, 61A and 62). In addition, in most cases, only very impulsive phase arrivals were utilized for P-wave polarities and for SV/P amplitude ratios.

The focal mechanism investigation followed 4 steps for each of the velocity models under consideration. First, the 14 impulsive polarity data points from event 61A, the 3.0 magnitude event of November 5, 1980, were analyzed by themselves. Next, the 1 amplitude ratio for that event was included. All of the impulsive polarities were then plotted on the event 61A solution. This step tested how well the event 61A solution explained the reliable polarities from the rest of the well-located events. Finally, a composite of events 42B and 42C (2 events very close together in space and time) was tested using both the SV/P amplitude ratios and the polarity data. The arrivals for these two events were less impulsive, so the polarity data is not as reliable as the event 61A polarities; however, the arrivals were strong enough to allow picking a first motion with a reasonable level of confidence. This latter procedure allowed comparison of an independent solution with that for event 61A.

The above focal mechanisms were first obtained for the events as located by the discrete layer model (Model 1). When just the event 61A polarity data is used, a large number of possible solutions are returned (Figure 18). When the 1 amplitude ratio is included with the polarities, a single solution is returned for 1 error in the polarities (Figure 19). This solution implies normal faulting with nodal planes striking northwest and dipping to the south and northeast. Notice that the northeast dipping plane, in particular, is not well constrained by polarity data.

Figure 18: Event 61A Focal Mechanisms Model 1 Determined from P-wave PolarityData

Event 61A possible sets of B, P and T axes using the azimuths and take-off angles as calculated by HYPOELLIPSE for Model 1 and constrained only by the P-wave polarity data. These are the solutions for 1 error in the P-wave polarities.

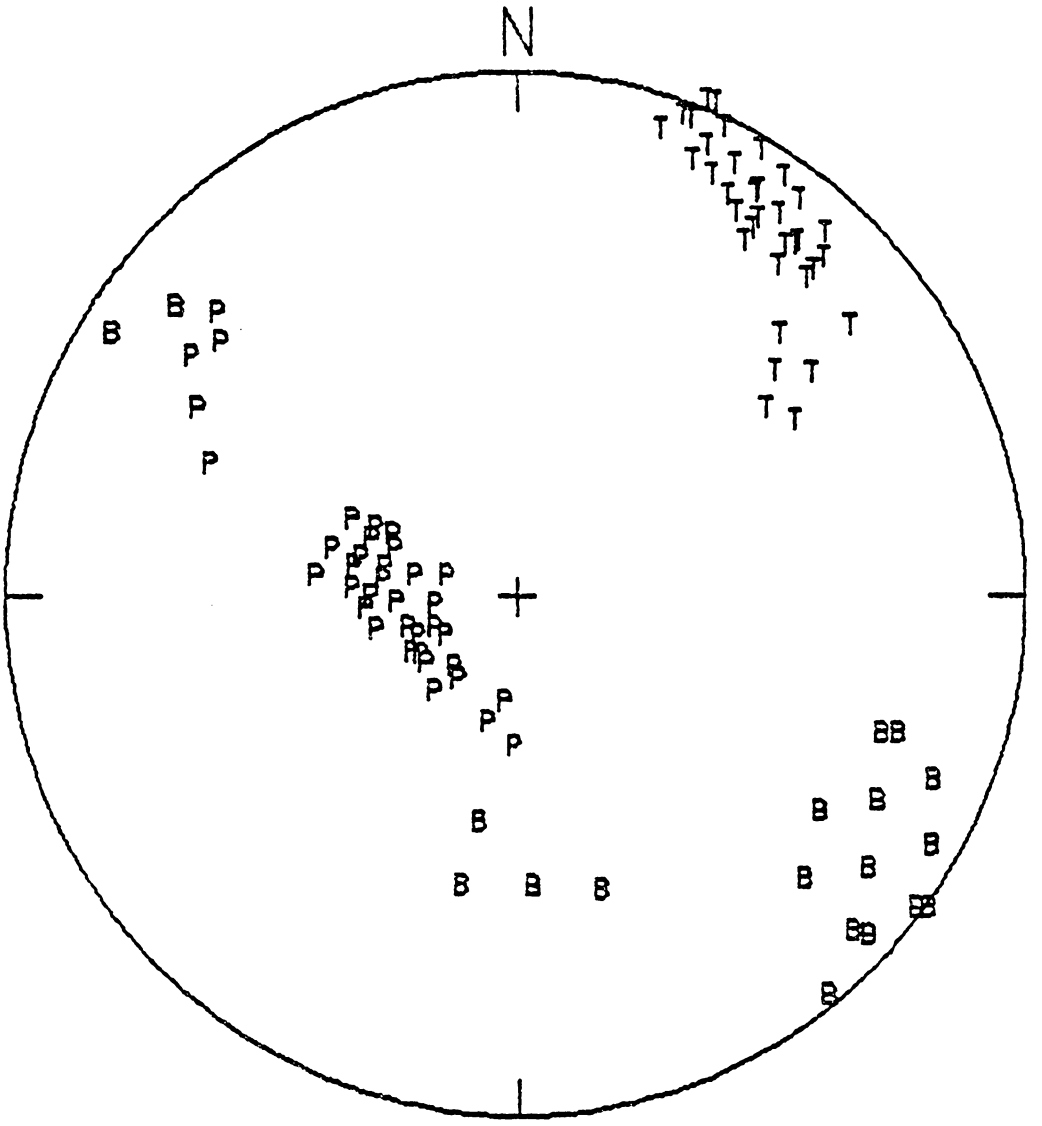
N

Figure 19: Event 61A Focal Mechanism Model 1 Determined from P-wave Polarity and SV/P Amplitude Data

Event 61A focal mechanism solution for Model 1 azimuths and take-off angles using P-wave polarities and the SV/P amplitude ratio. This is the solution for 1 error in the polarities and no errors in the amplitude ratios.

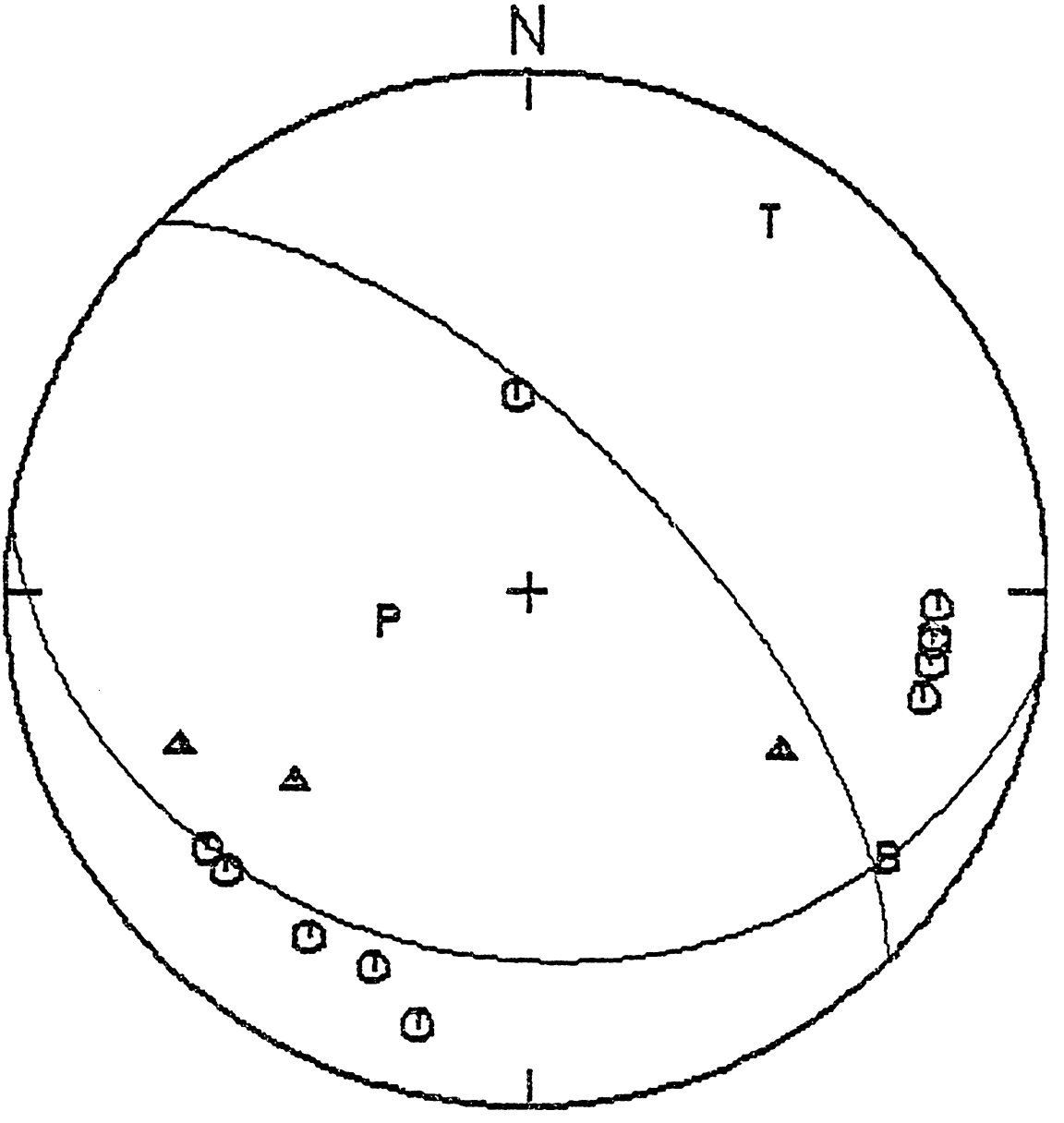
N
T
P

Next, all of the reliable P-wave polarities (24 from the 5 events) were plotted on the event 61A solution that was constrained by the amplitude ratio. If all of the events have a similar mechanism, which may be suspected from the events lineation, then the P-wave polarities from all of the events should plot in the proper quadrant on the event 61A solution. Four of the additional 10 impulsive polarities plot in the incorrect quadrant, yielding a total of 5 out of 24 (20%) inconsistencies for the composite (Figure 20).

For the event 42B and 42C composite, no solution was found for less than 28% inconsistencies in the polarity data and 40% inconsistency in the amplitude ratio data. This was considered excessive, so the solution was rejected.

The above procedure was applied to the events as located by the gradient over layer over mantle model (Model 3). Using just the event 61A polarities again, the program returned many solutions (Figure 21). When the 1 amplitude ratio is included, a single solution is returned for 2 errors in the polarities. This solution implies a combination of strike-slip and reverse faulting (Figure 22). The nodal planes strike approximately east-west and north-south. The east-west striking plane dips to the south as it did in the solution obtained using Model 1. The 10 remaining impulsive polarities plot on the event 61A solution with only 2 errors (Figure 23). This yields a composite inconsistency of 16%.

Figure 20: Plot of Reliable P-wave Polarity Data on the Event 61A Solution

This figure shows all of the impulsive polarities (24 from the 5 events) plotted on the event 61A solution shown in Figure 19. The composite has 5 out of 24 (20%) inconsistencies.

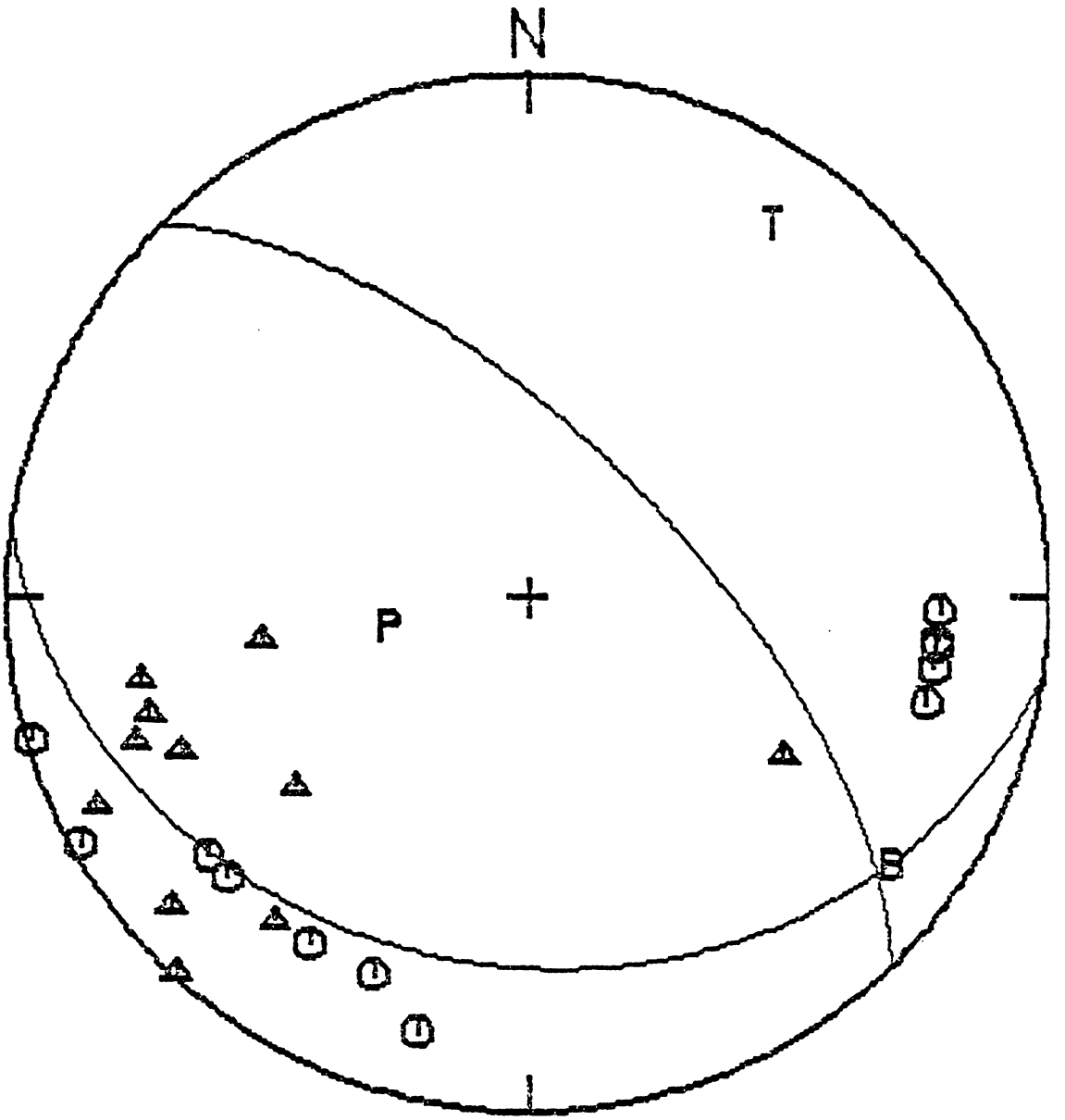
N
T
P

Figure 21: Event 61A Focal Mechanisms Model 3 Determined from P-wave Polarity Data

Possible sets of B, P and T axes for event 61A using Model 3 azimuths and take-off angles. Only the P-wave polarities are used and these solutions are for 1 error in the polarity data.

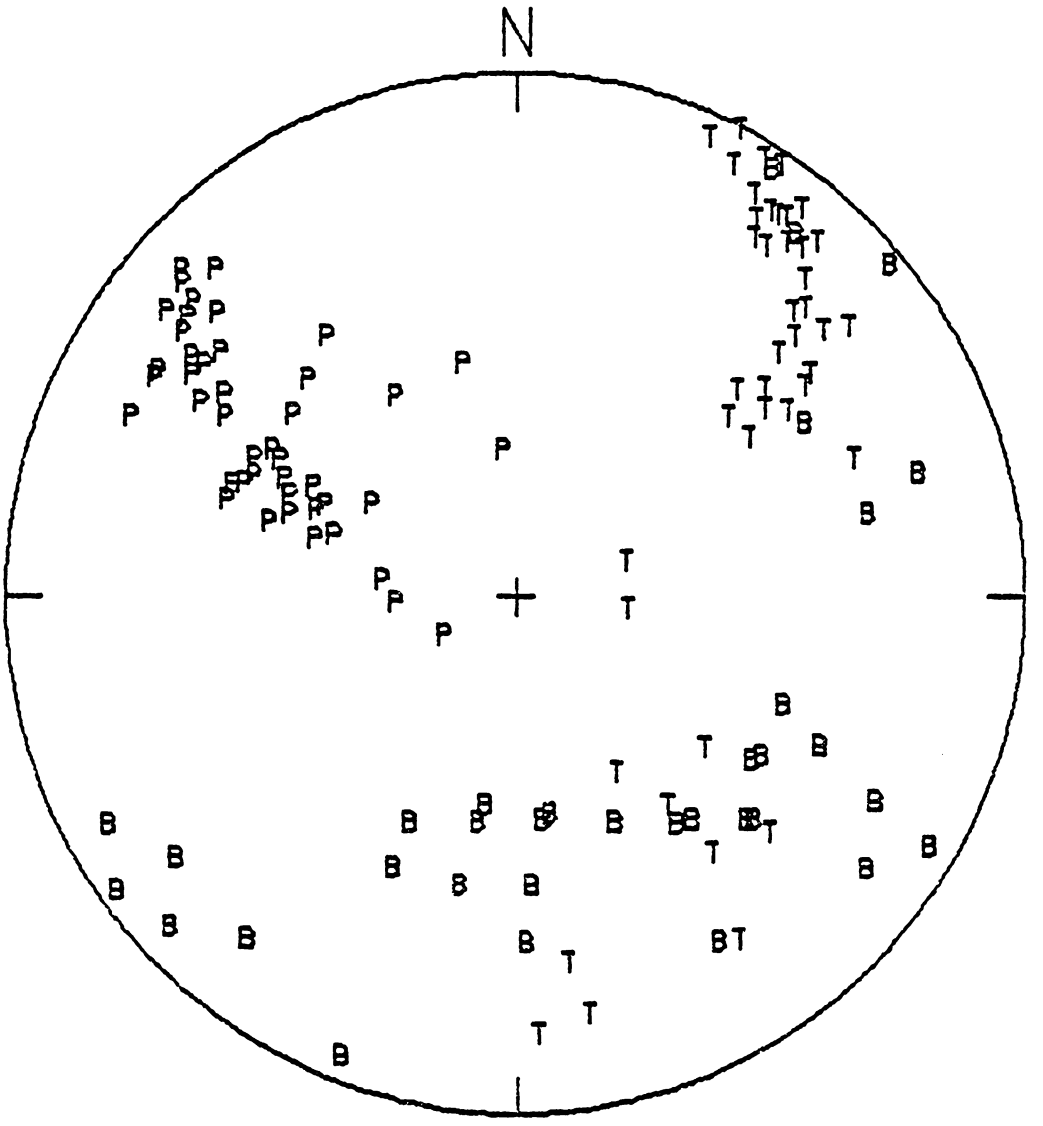
N

Figure 22: Event 61A Focal Mechanism (P-wave Polarity Data SV/P Amplitude Data) Model 3

Event 61A focal mechanism solution for Model 3 azimuths and take-off angles using P-wave polarities and the SV/P amplitude ratio. This solution is for 2 errors in the polarity data and no errors in the amplitude ratio data.

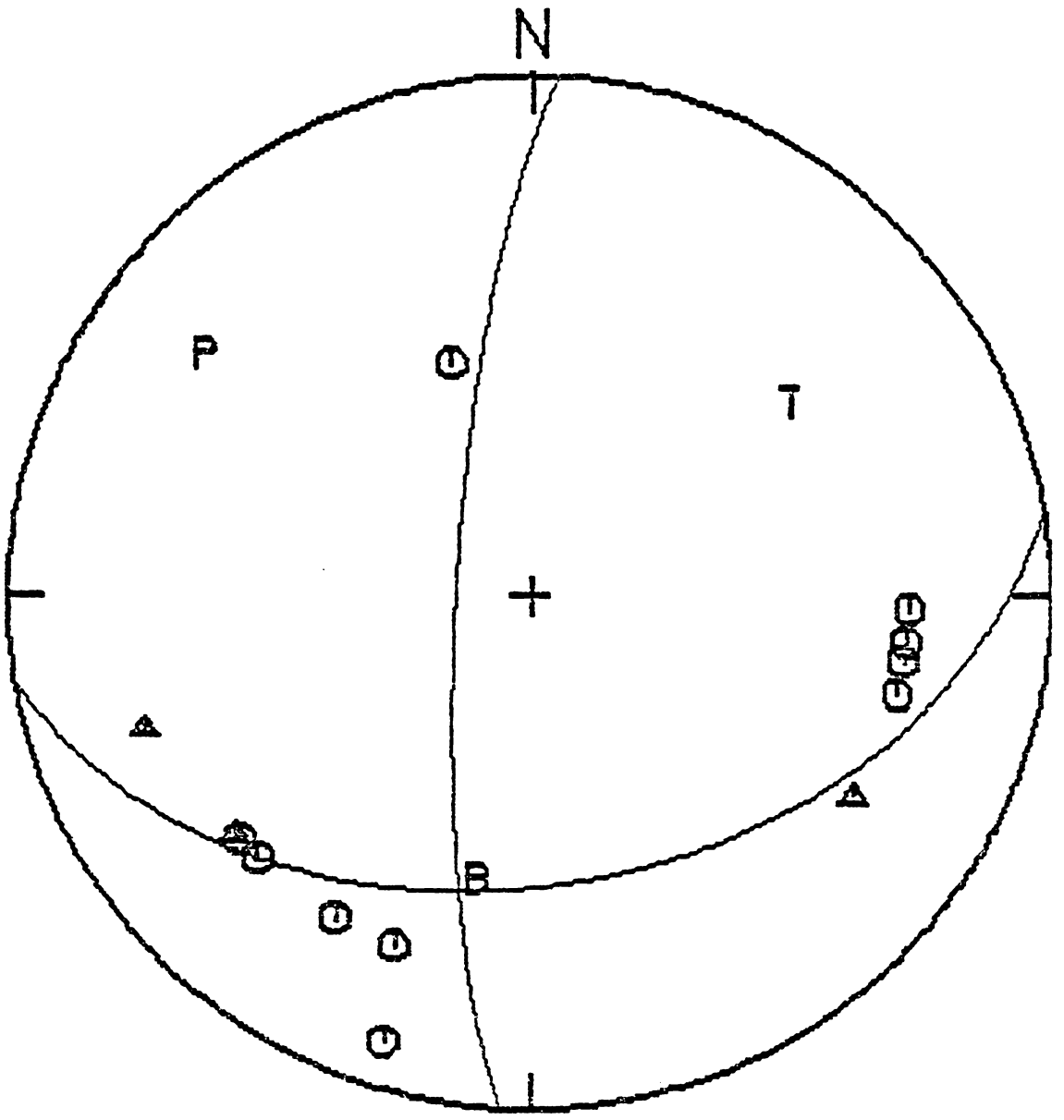
N
P
T
B

Figure 23: Plot of Reliable Polarity Data on the Event 61A Solution

This figure shows all of the impulsive polarity data plotted on the event 61A solution shown in Figure 22. The composite has 4 out of 24 (16%) inconsistencies.

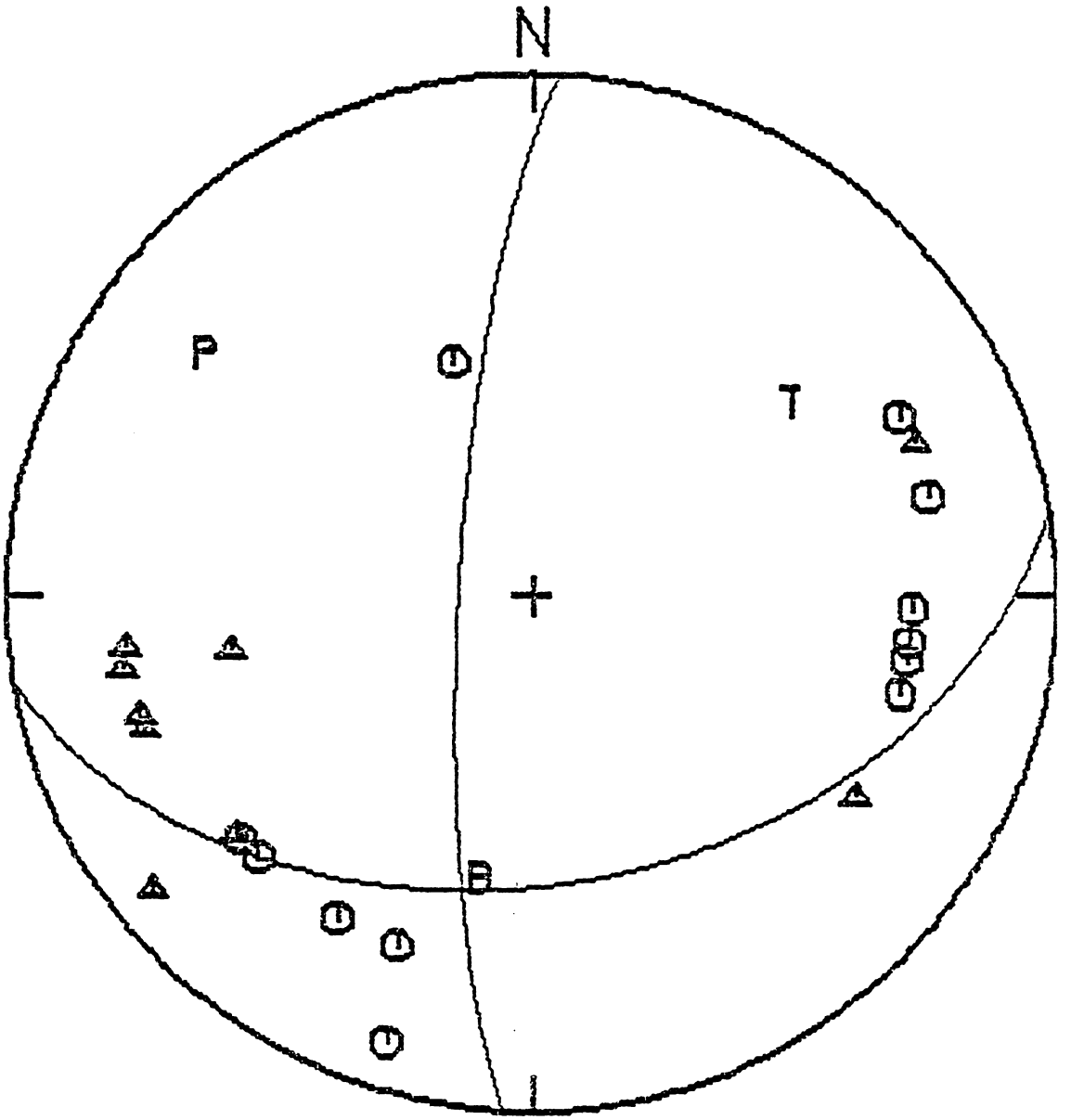
N
P
T
B

Finally, events 42B and 42C were composited. A single solution was found when 3 polarity errors out of 16 (18%) and 1 amplitude ratio error out of 4 (25%) was allowed. The solution (Figure 24) is a predominately reverse fault and is similar to the event 61A solution for this model. The nodal planes are rotated approximately 15 degrees counterclockwise.

In summary, the focal mechanism study has shown the following. For both velocity models, reliable solutions give one nodal plane striking east-west and dipping to the south. Since the events form an east-west trending lineament, an east-west striking fault plane or planes dipping to the south is a possible explanation for the activity. The exact mechanism is, however, undetermined, because normal faulting is indicated by Model 1 and strike-slip faulting by Model 3. Strike-slip mode is perhaps the more likely due to the fact that almost identical solutions were found for event 61A and the composite of events 42B and 42C for Model 3, whereas no solution was found for the 42B and 42C composite for Model 1. In addition, the predominately strike-slip faulting of this solution agrees with the combination strike-slip and reverse faulting that is expected by the stress regime in the Mid-continent region (Zoback and Zoback, 1980). Since the focal mechanisms derived from Model 3 azimuths and angles of incidence yield results that are consistent with this study, Model 3 is probably doing a better job of event location than Model 1.

Figure 24: Composite Focal Mechanism Solution for Events 42B and 42C (Model 3)

Events 42B and 42C composite focal mechanism solution using Model 3 azimuths and take-off angles. This solution is for 3 out of 16 inconsistencies (16%) in the P-wave polarities and 1 out of 4 (25%) inconsistencies in the amplitude ratio data.

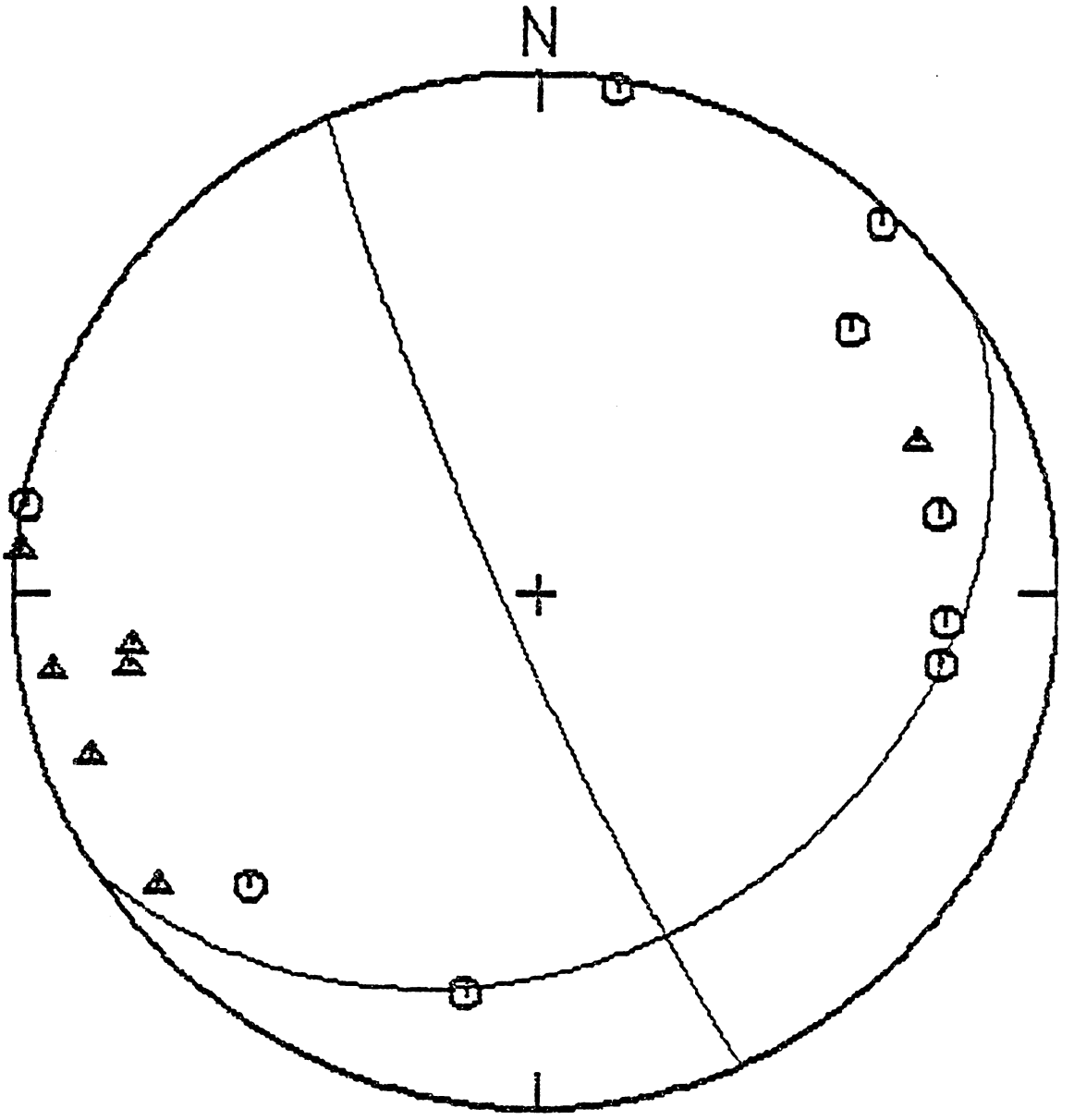
N

Chapter V

SUMMARY AND CONCLUSIONS

The crustal velocity in the Bath County Network locale can be represented by two equally likely models. The first model is a discrete velocity layer model (Model 1). This model uses the upper crustal P and S velocities derived from the blast monitoring done in this study and the lower crustal velocities derived in other studies of Virginia. The second model uses a linear velocity gradient with P velocity extending from 5.45 km/sec at the surface to 6.05 km/sec at 14.7 km depth (Model 3). The surface value of the VP/VS ratio is assumed for this entire layer. Under this layer, the discrete lower crustal velocities previously derived in Southwest Virginia are again used. The above crustal velocity models both produce epicentral locational errors of less than 1 km inside the network and some 3 km outside the network. The depth control inside the network is good with the depth error averaging less than 1 km. Outside the network depth control is poor to absent.

The above two velocity models were used to locate network recorded events and gave virtually identical results. Overall, the ellipse qualities ranged from A to D. The events tend to form an east-west lineation that extends for approximately 80 km. The reliable focal mechanisms obtained yield a solution with an east-west striking nodal plane that dips to the south. Since the events also trend east-west, that no-

dal plane is to be preferred as a possible fault plane or planes. The other nodal plane, that in effect defines the mode of faulting, is not constrained. That is, its orientation depends on which of the two possible velocity models are used.

A low level of seismicity classifies this area as virtually aseismic. That aseismic character is established by the low level of seismicity detected by network monitoring, the lack of events detected during field monitoring and the historical record.

REFERENCES

Bollinger, G.A. (1977). Reinterpretation of the intensity data for the 1886 Charleston, S.C. earthquake, in D.W. Rankin, ed. Studies related to the Charleston, S.C. earthquake of 1886 - A preliminary report, USGS Prof. paper 1028, pp. 17-32.

Bollinger, G.A. (1975). A catalog of southeastern United States earthquakes - 1754 through 1974: Research Division Bulletin 101, Virginia Polytechnic Institute and State University, 68 p.

Bollinger, G.A. and M.C. Gilbert (1974). A reconnaissance microearthquake survey of the Hot Springs, Virginia Area, Bull. Seis. Soc. Am., 64, December 1974, pp. 1715-1720.

Borcherdt, R.D. and J.C. Roller (1966). A preliminary summary of a seismic-refraction survey in the vicinity of the Cumberland Plateau Observatory, Tennessee, U.S. Geological Survey Technical Letter No. 43, 21 p.

Bullen, K.E. (1947). An Introduction to the Theory of Seismology, Cambridge University Press, London, 381 pp.

Butts, C. (1933). Geologic map of the Appalachian Valley in Virginia, VDMR Geologic map.

Butts, C. (1940). Geology of the Appalachian Valley in Virginia, Virginia Geol. Surv. Bull., 52, part 1, 68 p.

Carts, D.A. (1981). A regional crustal velocity model for the southeastern United States, Virginia Polytechnic Institute and State University, M.S. Thesis, 124 p.

Chapman, M.C. (1979). Seismic velocity structure of central Virginia, Virginia Polytechnic Institute and State University, M.S. Thesis, 146 p.

Colton, G.W. (1970). The Appalachian basin - its depositional sequences and their geological relationships, Studies of Appalachian Geology: Central and Southern, Interscience Publishers, New York, pp. 5-47.

Dennison, J.M. and R.W. Johnson, Jr. (1971). Tertiary intrusions and associated phenomena near the thirty-eighth parallel fracture zone in Virginia and West Virginia, Bull. Geol. Soc. Am., 82, pp. 501-508.

Dobrin, M.B. (1976). Introduction to Geophysical Prospecting, McGraw-Hill, New York, 630 p.

Dorman, L.M. (1972). Seismic crustal anisotropy in northern Georgia, Bull. Seis. Soc. Am., 62, pp. 39-45.

Dutton, C.E. (1889). The Charleston earthquake of August 31, 1886, Annual Report, USGS 1887-88, pp. 209-528.

James, D.E., T.J. Smith and J.C. Steinhart (1968). Crustal structure of the middle Atlantic states, J. Geop. Res., 73, pp. 1983-2007.

Kulander, B.R. and S.L. Dean (1978). Gravity, magnetics, and structure of the Allegheny Plateau/Western Valley and Ridge in West Virginia and adjacent states, West Virginia Geological and Economic Survey Report of Investigation RI-27, 91 p.

Lahr, J.C. (1980). HYPOELLIPSE/MULTICS: A computer program for determinig local earthquake hypocentral parameters, magnitude, and first motion pattern, U.S. Geological Survey Open-File report 80-59, revised April 1980, for version II, 59 p.

Lee, W.H.K. and S.W. Stuart (1981). Advances in Geophysics, Supplement 2, Principles and Applications of Microearthquake Networks, Academic Press, New York, 273 p.

Lowry, W.D. (1973). Striking differences in the structural development of the southern and central Appalachians of Virginia, Geol. Soc. Am. Abstr. with Programs, 5, pp. 719-720.

Moore, T.P. (1979). Crustal velocity structure in southwestern Virginia, Virginia Polytechnic Institute and State University, M.S. Thesis, 75 p.

Perry, L. D., J. K. Costain and P. A. Geiser (1979). Heat Flow in Western Virginia and a Model for the Origin of Thermal Springs in the Folded Appalachians, J Geop. Res., 84. pp. 6875-6883

Richter, C.F. (1958). Elementary Seismology, W.H. Freeman and Company, San Francisco, 768 p.

Simpson, D.W. (1976). Seismicity changes associated with reservoir loading, Eng. Geol., 10, Amsterdam, pp. 123-150.

Steinhart, J.S. and R.P. Meyers (1978). Explosion Studies of Continental Structure, Carnegie Inst. of Wash. Publications 622, Washington, D.C., 409 p.

Tzeng, W.S. (1982). Investigation of SV to P wave amplitude ratio for determining focal mechanism, Georgia Institute of Technology, M.S. Thesis, 78 p.

Zoback, M.L. and M. Zoback (1980). State of stress in the conterminous United States, J. Geop. Res., 85, pp. 6113-6156.

Appendix A

BLAST ARRIVAL AND TRAVEL TIMES

Station	Date mo/day/yr	Phase	Arrival Time hr:min:sec	Travel Time sec
TWR	06/24/82	P	21:35:01.2	0.65
GUY	06/24/82	P	21:35:03.2	2.00
GUY	06/24/82	S	21:35:04.2	3.00
BV3	06/24/82	P	21:35:02.3	1.10
BV2	06/24/82	P	21:35:04.0	2.80
TWR	06/25/82	P	21:43:25.6	0.70
GUY	06/25/82	P	17:35:08.9	2.05
GUY	06/25/82	S	17:35:09.8	2.95
GUY	06/25/82	P	21:43:27.0	2.10
GUY	06/25/82	S	21:43:28.1	3.20
STH	06/25/82	P	21:43:26.75	1.85
HVP	06/25/82	P	21:43:27.5	2.60
BV3	06/25/82	P	17:35:08.0	1.15
BV3	06/25/82	P	21:43:26.0	1.10
BV2	06/25/82	P	17:35:08.7	2.75
BV2	06/25/82	P	21:43:27.5	2.60
STH	06/26/82	P	21:28:50.5	1.70
HVP	06/26/82	P	21:28:51.3	2.50
HVP	06/26/82	S	21:28:53.3	4.50
TWR	06/26/82	P	18:02:20.0	0.65
TWR	06/26/82	P	21:28:49.5	0.70

Station	Date mo/day/yr	Phase	Arrival Time hr:min:sec	Travel Time sec
GUY	06/26/82	P	18:02:21.15	1.80
GUY	06/26/82	S	18:02:22.1	2.75
GUY	06/26/82	P	21:28:50.6	1.80
BV3	06/26/82	P	18:02:20.5	1.15
BV3	06/26/82	P	21:28:49.8	1.00
BV2	06/26/82	P	18:02:21.9	2.55
BV2	06/26/82	P	21:28:51.2	2.40
HVP	06/28/82	P	21:41:27.0	2.60
HVP	06/28/82	S	21:41:28.5	4.10
GUY	06/28/82	P	21:41:26.3	1.90
GUY	06/28/82	S	21:41:27.9	3.00
TWR	06/28/82	P	21:41:25.05	0.65
TWR	06/29/82	P	17:04:26.15	0.65
TWR	06/29/82	P	21:51:53.6	0.65
GUY	06/29/82	P	17:04:27.4	1.90
GUY	06/29/82	S	17:04:28.2	2.70
GUY	06/29/82	P	21:51:54.85	1.90
GUY	06/29/82	S	21:51:55.9	2.95
HVP	06/29/82	P	17:04:28.05	2.55
HVP	06/29/82	P	21:51:55.5	2.55
HVP	06/29/82	S	21:51:56.9	3.95
TWR	06/30/82	P	22:25:37.0	0.65
GUY	06/30/82	P	22:25:38.2	1.85
GUY	06/30/82	S	22:25:39.1	2.75

Station	Date mo/day/yr	Phase	Arrival Time hr:min:sec	Travel Time sec
HVP	06/30/82	P	22:25:38.9	2.55
HVP	06/30/82	S	22:25:40.6	4.25
TWR	07/01/82	P	18:05:51.0	0.65
TWR	07/01/82	P	22:27:01.6	0.65
GUY	07/01/82	P	18:05:52.2	1.85
GUY	07/01/82	S	18:05:53.2	2.85
GUY	07/01/82	P	22:27:02.8	1.85
GUY	07/01/82	S	22:27:03.8	2.85
CEM	07/01/82	P	18:05:52.4	2.05
BEN	07/01/82	P	18:05:51.5	1.15
BEN	07/01/82	S	18:05:52.3	1.95
BEN	07/01/82	P	22:27:02.1	1.15
BEN	07/01/82	S	22:27:02.8	1.85
CEM	07/02/82	P	16:12:29.3	2.15
CEM	07/02/82	P	21:44:18.4	2.10
CEM	07/03/82	P	16:10:52.1	2.15
BEN	07/03/82	P	16:10:51.2	1.25
BEN	07/03/82	S	16:10:52.0	2.05
CEM	07/06/82	P	16:28:08.0	2.10
CEM	07/06/82	P	21:42:16.95	2.10
BEN	07/06/82	P	16:28:07.0	1.10
BEN	07/06/82	P	21:42:15.9	1.05
BEN	07/06/82	S	21:42:16.7	1.85
MGC	07/16/82	P	16:19:56.6	2.85

Station	Date mo/day/yr	Phase	Arrival Time hr:min:sec	Travel Time sec
614	07/16/82	S	16:19:58.3	4.55
614	07/19/82	S	21:42:47.2	4.50
614	07/19/82	S	21:48:20.6	4.00
DCR	07/19/82	P	21:42:45.9	3.20
DCR	07/19/82	P	21:48:19.9	3.30
PCG	07/19/82	P	21:42:46.2	3.55
PCG	07/19/82	S	21:42:48.6	5.90
PCG	07/19/82	P	21:48:20.2	3.60
PCG	07/19/82	S	21:48:23.0	6.40
614	07/20/82	S	21:41:04.2	4.25
DCR	07/20/82	P	21:41:03.1	3.15
PCG	07/20/82	P	21:41:03.5	3.55
PCG	07/20/82	S	21:41:05.8	5.85
614	07/21/82	S	16:13:31.3	4.60
614	07/21/82	S	21:39:27.2	4.05
DCR	07/21/82	P	16:13:30.0	3.30
PCG	07/21/82	P	16:13:30.3	3.60
PCG	07/21/82	S	16:13:33.0	6.30
PCG	07/21/82	P	21:39:26.9	3.75
PCG	07/21/82	S	21:39:29.7	6.55
614	07/22/82	S	21:38:37.9	4.95
DCR	07/22/82	P	16:28:19.2	3.35
614	07/23/82	S	16:18:36.3	4.70
DCR	07/23/82	P	16:18:34.9	3.30

Station	Date mo/day/yr	Phase	Arrival Time hr:min:sec	Travel Time sec
PCG	07/23/82	P	16:18:35.2	3.60
MGC	07/26/82	P	21:42:22.3	3.00
MGC	07/27/82	P	21:51:10.4	3.05
HAY	08/06/82	P	16:25:04.6	3.70
HAY	08/10/82	P	21:56:49.6	3.60
HAY	08/10/82	S	21:56:52.4	6.42
HAY	08/11/82	S	21:40:40.8	6.95
CRF	08/11/82	P	21:40:38.8	5.95
HAY	08/12/82	P	16:20:42.3	3.70
CRF	08/12/82	P	16:20:44.55	5.95
HAY	08/13/82	S	16:12:05.5	6.70
CRF	08/16/82	P	21:42:40.35	5.95
MFH	08/16/82	P	16:16:24.15	6.25
MFH	08/16/82	P	21:42:40.8	6.45

The vita has been removed from the scanned document

SEISMICITY OF THE BATH COUNTY, VIRGINIA LOCALE

by

Eric Donald Todd

(Abstract)

Thirty-nine construction blasts were monitored by mobile and fixed seismic arrays to develop a crustal velocity model in the Bath County, Virginia locale (June-August, 1982). The results indicate an upper-layer with P and S velocities of 5.45 km/sec and 3.07 km/sec respectively, and a thickness 3 km. Data from the 2 most distant observing stations indicate a second layer with a P velocity of 6.04 km/sec. Based on other studies in Virginia, lower crustal layers with P and S velocities 6.05 km/sec and 3.52 km/sec (11.7 km thickness) and 6.53 km/sec and 3.84 km/sec (36.0 km thickness) and upper mantle velocities of 8.18 km/sec and 4.79 km/sec are assumed. These layers make up the discrete velocity layer model. The observed travel-time data cannot be distinguished from theoretical travel-times calculated from either of two other models utilizing linear increases in velocity with depth. The first of these models uses a linear increase in P velocity from 5.45 km/sec at the surface to 6.53 km/sec at 50.7 km depth. The surface VP/VS ratio of 1.74 is assumed for this entire layer. Beneath this layer is the mantle with P and S velocities 8.18 km/sec and 4.79 km/sec. The second of these models uses a linear increase in P velocity from 5.45 km/sec at the surface to 6.05 km/sec at 14.7 km depth. The surface VP/VS ratio is again assumed for this layer. Beneath this layer is the 36.0 km thick 6.53 km/sec layer underlain by the mantle.

A test of the locational capabilities of the Bath County Network utilizing construction and quarry blasts was carried out for the 3 different velocity models. All three models gave virtually identical locations. The tests indicate an average of less than 1 km epicentral and depth errors inside the network. On the edge of the network, accuracy degrades to 3 km epicentral error with poor depth control.

The Bath County area is seismically quiescent. Portable seismographs recorded over 3,000 hours of low noise seismic data in June, July and August of 1982 and failed to detect any local earthquake activity. Network monitoring by a permanent 4 station microearthquake network from November 1978 to November 1982 resulted in 11 recorded events. Three of these events were too small to be located. The other 8 events were located using all 3 velocity models. The linear increase in velocity over mantle model was eliminated from further consideration due to poor performance in event location. The other two model gave virtually identical locations. For these two models, the events form an apparent east-west trend. Reliable focal mechanisms, using both P wave polarities and SV/P amplitude ratios, indicate one nodal plane striking east-west and dipping to the south. The other nodal plane, which defines the mode of faulting, is poorly constrained.